Research article

Bimolecule detection for Extracellular Vesicle Screening

Hisako Kaneda[1, 2], Yui Ida[1], Ryusuke Kuwahara[3], Izumi Sato[1], Takanari Nakano[1], Haruhiko Tokuda[4], Tsuyoshi Sato[2], Takayuki Murakoshi[1], Koichi Honke[5], and Norihiro Kotani[1*]

[1]Department of Biochemistry, Saitama Medical University, 38 Morohongo, Moroyama-machi, Iruma-gun, Saitama, 350-0495, Japan

[2]Department of Oral and Maxillofacial Surgery, Saitama Medical University, 38 Morohongo, Moroyama-machi, Iruma-gun, Saitama, 350-0495, Japan

[3]Quantum Wave Microscopy Unit, Okinawa Institute of Science and Technology Graduate University, 1919-1 Tancha, Onna-son, Kunigami-gun, Okinawa, 904-0495, Japan

[4]Medical Genome Center Biobank, National Center for Geriatrics and Gerontology, 7-430 Morioka-cho, Obu, Aichi, 474-8511, Japan

[5]Department of Biochemistry, Kochi University Medical School, Nankoku, Kochi, 783-8505, Japan

*To whom correspondence should be addressed: Norihiro Kotani: Department of Biochemistry, Saitama Medical University, 38 Morohongo, Moroyama-machi, Iruma-gun, Saitama 350-0495, Japan; kotani@saitama-med.ac.jp; Tel: +81-49-276-1155; Fax: +81-49-276-1155 ORCID ID: 0000-0003-3739-6478

Abstract

Extracellular vesicles (EVs) have been investigated for use in clinical testing in recent years. Specific EV surface proteins provide distinguishing characteristics, but are insufficient for more detailed classification of EVs. Here, we suggest a novel "Bimolecular surface antigen expressed in EV" (BiEV) as a potential indicator for more efficient EV screening. A BiEV can be identified using a proximity labeling method applicable to EV membrane proteins. We examined the screening of BiEV in cancer cell-secreted EV included in serum EVs from a model mouse for lung cancer, showing that the CHL1-SLC4A1 BiEV was a significant candidate. ELISA quantification of CHL1-SLC4A1 BiEV appeared to suggest a potential for cancer screening of these mice. Using the same protocols, we found that CHL1-caspase 14 BiEV was significantly elevated in lung cancer patients. A BiEV strategy may be able to make a contribution to more effective EV screening, resulting in novel clinical applications.

Introduction

Extracellular vesicles (EVs) are lipid membrane vesicles 40 to 1000 nm in size secreted extracellularly by various cells. They are classified into several types based on their properties, secretory processes, and size (Cocucci and Meldolesi, 2015; Raposo and Stoorvogel, 2013; Van Niel et al., 2018). Exosomes measuring approximately 50–150 nm and secreted through a multivesicular endosome contribute to not only the secretion of intracellular molecules, but also the transmissive mechanism that transports them to other cells for intercellular communication (Cocucci and Meldolesi, 2015; Raposo and Stoorvogel, 2013; Van Niel et al., 2018). Because EVs are secreted from various cells and possess a variety of properties, it is important to distinguish among them. Serum EV screening in particular is a valuable clinical tool and provides an alternative to serum proteins secreted from cancer cells. As a result, attempts are being made to diagnose various diseases by classifying and detecting disease-specific EVs (Shah et al., 2018). To our knowledge, the most recent advanced strategy involves the detection of non-coding RNAs (*e.g.*, miRNAs) in EVs (Anfossi et al., 2018), which may be able to detect large numbers of cancers with fairly high accuracy. Similarly, specific EV surface proteins expressed in these EVs (generally membrane proteins and/or membrane-attached proteins) have been investigated as targets for cancer screening (Xu et al., 2018). Their potential to be used as indicators for the characterization of EVs has been investigated using single surface proteins. However, many of these single proteins, including marker proteins for EVs, are known to be ubiquitous proteins, and as such may be insufficient for distinguishing and classifying EVs.

Cell membrane or membrane-attached proteins non-randomly form heterocomplexes accompanied by a fluid biological membrane known as a "lipid raft" structure (Brown and London, 1998). We reported that the membrane heterocomplex "Bimolecular Cancer Target" (BiCAT) could be a potential lung cancer (LC) antigen consisting of a hetero bimolecular complex (Kotani et al., 2019). In the BiCAT strategy, because cancer specific-antigens are defined by two molecules, the specificity is theoretically higher than that of a single-molecule antigen. Because EVs are composed of a lipid bilayer biological membrane, a heterocomplex, including a bimolecule, was considered to be an attractive indicator antigen to distinguish EVs.

To employ bimolecules in EV screening, it is essential to identify which molecules form the specific bimolecules in EVs. Proximity labeling (Kim and Roux, 2016; Rees et al., 2015) have recently attracted research resources to analyze these bimolecules. Among them, we developed a simple and physiological method, called enzyme-mediated activation of radical source (EMARS) (Kotani et al., 2008; Miyagawa-Yamaguchi et al., 2015), that labels only bimolecular partner proteins with fluorescein followed by analysis using an antibody array and/or typical proteome strategy (Jiang et al., 2012). To date, EMARS has been applied to various studies involving molecular complexes on cell membranes (Hashimoto et al., 2012; Ishiura et al., 2010; Iwamaru et al., 2016; Kaneko et al., 2016; Kotani et al., 2012; Ohkawa et al., 2015; Yamashita et al.,

2011).

Here, we propose a "Bimolecular surface antigen expressed in EV" (BiEV) as a new type of indicator to provide diversity in EV screening. Transgenic mice with *EML4-ALK* onco-fusion genes (Soda et al., 2008, 2007) were used as an animal model for the spontaneous onset of LC. We focused on BiEVs in cancer cell-secreted EVs (cEVs) of this mouse model, which includes exosomes and ectosomes, raised from several LC cell pathways resulting in secreted to serum. In addition, serum EVs derived from 12 serum samples of healthy persons and LC patients were purified and used for BiEV analysis by the same protocols. The experiments revealed specific BiEV antigens in both mouse and human LC cell-secreted EVs, suggesting that BiEV in cEVs can serve as indicators in EV screening and biomarkers for LC screening.

Materials and methods

Animals

C57BL/6J mice used as wild type mice were obtained by self-breeding of the pair mice purchased from Japan CLEA Co. (Tokyo, Japan), and were maintained under specific pathogen-free conditions (SPF) at 20-25 °C in accordance with the Saitama Medical University Animal Experiment Committee (protocol number 30M059). The *EML4-ALK* transgenic mice (Soda et al., 2008) (generous gift from Professor Hiroyuki Mano and Dr. Manabu Sone, National Cancer Center Research Institute) were maintained under SPF conditions at room temperature in accordance with Saitama Medical School Animal Experiment Committee (protocol number 2697 and 2701) and the Saitama Medical University Safety Committee for Recombinant DNA Experiments (protocol number 1356). All animals were maintained under a 12 hour light/12 hour dark exposure and free access to food and water.

Human serum samples

The serum samples of healthy persons and lung cancer patients were obtained from the Medical Genome Center Biobank, National Center for Geriatrics and Gerontology and BioBank Japan Project supported by Japan Agency for Medical Research and Development (AMED) (Hirata et al., 2017; Nagai et al., 2017) in Japan. The handling of human serum and its use in research are performed in accordance with the permission and the guidelines of the Ethics Review Committee of Saitama Medical University (protocol number 850).

Cell culture and EV isolation

The LK2 human squamous cell lung carcinoma cell lines (RIKEN CELL BANK, Ibaragi, Japan) were cultured in RPMI 1640 medium (Wako Chemicals, Osaka, Japan) supplemented with 5% fetal bovine serum (FBS; GIBCO) at 37°C under humidified air containing 5% CO_2. For the collection of secreted EVs from LK2 cells, the medium was replaced with new serum free medium, ASF Medium 104 (Ajinomoto, Tokyo, Japan), and then cultured cells continuously cells for 2 days. The secreted EVs were partially purified from cultured medium by using ExoQuick-TC Exosome Precipitation Solution (20 µl/100 µl serum; System Biosciences, CA) at 4°C for overnight. The precipitation containing EVs was solubilized with 100 µl PBS, and then used for further analysis.

Preparation of HRP-conjugated antibody for EMARS reaction

The mouse and human anti-CHL1 antibodies (AF2147 and MAB2126; R&D systems, MN) were partially reduced and bound to HRP using a peroxidase labeling kit SH (Dojindo, Kumamoto, Japan). The binding capacity of the HRP-labeled antibody was evaluated as described previously (Kotani et al., 2019).

Purification and EMARS reaction for serum EVs

The serum EVs from mouse and human serum were purified by using the combination of polymer precipitation and size exclusion chromatography. In order to determine which fractions should be collected for EV purification in size exclusion chromatography, mouse serum and blue dextran (Sigma-Aldrich Japan, Tokyo, Japan) were subjected to the short column with 2 ml Sephacryl S-500 resin (GE Healthcare Life Sciences, IL) equilibrated with PBS. The resins were pre-treated with yeast extract solution (0.1 g/100 ml H_2O for 1 hour; BD Biosciences, NJ) to avoid non-specific binding of EVs to resins. Then, the sample fractions were eluted with 100 µl PBS/fraction. The protein concentration of each fraction was measured using micro BCA protein assay kit (Thermo Fisher Scientific, MA) with VarioSkan Flash microplate reader (Thermo Fisher Scientific, MA) at 562 nm. The blue dextran was measured by with VarioSkan Flash microplate reader at 300 nm.

The serum (50-100 µl) was treated with ExoQuick Exosome Precipitation Solution (25.2 µl/100 µl serum; System Biosciences, CA) on ice for 30 min. The precipitation (hereinafter referred to as precipitated EV) was solubilized with 100 µl PBS, and then added 0.25 µg of HRP-conjugated anti-mouse or human CHL1 antibody with gentle mixed. After incubation at room temperature for 20 min, the precipitated EV mixture was subjected to short column with 2ml Sephacryl S-500 equilibrated with PBS. The step-by-step elution was carried out under gravity flow with PBS (100 µl PBS/fraction). The fractions No. 6 to 8, which contained EVs with HRP-conjugated CHL1 antibody, were collected depend on each experiment, and applied to Nanosep® centrifugal devices (30K; Pall Life Sciences, MI) followed by centrifugation at 8,000 g for 5 min to concentrate EV particles. The concentrated EV particles on the filters were washed with 100 µl PBS once by centrifugation, and then fluorescein-tyramide (FT) reagent as EMARS reaction reagent (Kotani et al., 2019) was added to the filter with gentle mixing. After 10 min incubation at room temperature, remaining FT reagent was removed by centrifugation at 8,000 g for 5 min followed by wash with PBS once by centrifugation. The EV proteins after EMARS reaction on the filter were collected with 30 µl of 50 mM Tris-HCl (pH 7.4) containing 1% SDS by gentle pipetting and transferred to new tube. To remove excess FT reagent, the collected sample was subjected to mini column with approx. 1ml Sephadex G-50 (GE Healthcare Life Sciences, IL), which was equilibrated with 50 mM Tris-HCl (pH 7.4) containing 1% SDS. The eluted samples (approx. 30 µl) were subsequently used for the analysis of EMARS products, such as immunoprecipitation, western blot, and ELISA described below. In the case of direct detection of EMARS products on SDS-PAGE gel, the gel was directly subjected to ChemiDoc MP Image analyzer (BIO-RAD, CA) with the gel fluorescent detection mode (blue light filter for fluorescein). For loading controls, the gel after exposure was stained with Coomassie Brilliant Blue solution.

Cryo-electron microscopy

For cryoEM imaging of EVs, the grids were prepared by applying 3 µl sample on glow-discharged holey carbon grids (Quantifoil Mo 2/2 200 mesh). The sample was ice-embedded using a LEICA EM GP2 (Leica

Microsystems, Tokyo, Japan) at 100% humidity and 10 °C. Images were collected on an FEI Talos Arctica microscope (Thermo Fisher Scientific, MA) at 200 kV using a Falcon III detector in liner mode and a Volta phase plate. Each data was collected at a dose rate of $10e^{-}$/pixel/sec for 4 s, with a total accumulated dose of ~ 40 $e^{-}/Å^2$.

Purification and Enrichment of EMARS products

EMARS products were purified and enriched with anti-fluorescein antibody-conjugated Sepharose as described previously (Kotani et al., 2019). Briefly, the flow-through fraction of G-50 column described above was diluted with 300 µL of NP-40 lysis buffer. Then, 20 µl of prepared anti-fluorescein antibody Sepharose, which was produced by the conjugation reaction between anti-fluorescein antibody (600101096; Rockland Immunochemicals, PA or 6400-01; Southern Biotech, AL) and NHS-activated Sepharose 4 Fast Flow (GE Healthcare Life Sciences, IL), was added to the sample, and mixed with rotation at 4°C for overnight. After washing resins, appropriate solutions (reducing SDS-sample buffer for western blot or 1 % SDS solution containing MPEX PTS reagent (GL Science, Tokyo, Japan) for MS analysis) was added to Sepharose beads, and heated at 95°C for 5 min to elute the fluorescein-labeled molecules from resins.

Proteomic Analysis of EMARS products by using mass spectrometry analysis

Proteomic analysis in this study was performed by using nano liquid chromatography-electrospray ionization mass spectrometry (nano LC-ESI-MS/MS). In the case of proteomic analysis for BiEVs in mouse serum EVs, we received the technical support of MS analysis (Laboratory of Cytometry and Proteome Research, Nanken-Kyoten and Research Core Center, Tokyo Medical and Dental University). Briefly, the peptide samples of EMARS products derived from serum EVs were purified under same protocols as described above, and were injected into a nano-UHPLC system (Bruker Daltonics, MA). Mass analysis was performed on a maXis-4G-CPR (Bruker Daltonics, MA) mass spectrometer equipped with a nano-ESI source. An L-column ODS (0.1x150 mm, 3 µm particle size, CERI, Tokyo, Japan) was used, preceded by a Magic C18AQ UHPLC NanoTrap column (5 µm particle size, 200 Å pore diameter). The peptides were eluted from the column using a 10% to 35% acetonitrile gradient over 50 min. The eluted peptides were directly electro-sprayed into the spectrometer, with MS/MS spectra acquired in a data-dependent mode.

In the case of proteomic analysis for BiEVs in human serum EVs, we received the technical support of MS analysis (the Natural Science Center for Basic Research and Development (N-BARD), Hiroshima University). The peptide samples of EMARS products prepared as well as mouse samples were injected into an Ultimate 3000 RSLCnano (Thermo Fisher Scientific, MA). Mass analysis was performed on a LTQ Orbitrap XL mass spectrometer equipped with a nano-ESI source (Thermo Fisher Scientific, MA). A NIKKYO nano HPLC capillary column (3µm C18, 75 µm I.D.×120 mm; Nikkyo Technos) was used, preceded by a C18 PepMap100

column (300 μm I.D × 5mm; Thermo Fisher Scientific, MA). The peptides were eluted from the column using a 4% to 35% acetonitrile gradient over 97 min. The eluted peptides were directly electro-sprayed into the spectrometer, with precursor scan and data-dependent MS/MS scan.
The raw data was analyzed using Proteome Discoverer ver. 2.2 software (Thermo Fisher Scientific, MA) with the following parameters: Cys alkylation: iodoacetamide, Digestion: Trypsin, Species: Homo sapiens or Mus musculus, FDR (False discovery rate): strict 1%, relaxed 5%, respectively.

Western blot analysis

For western blot analysis, the solubilized samples (purified EVs etc.) with reducing SDS sample buffer or the eluted samples from purified and enriched resins described above were subjected to 6 to 12 % SDS-PAGE by using typical SDS-running buffer or Rapid Running Buffer Solution (Nacalai Tesque, Kyoto, Japan) in order to adjust to molecular mass of each candidate protein. The gels were subsequently blotted to an Immobilon®-P PVDF Membrane (Millipore, MA). After blocking with 5% skim milk solution, transferred membrane was reacted with first antibodies as follows: anti-fluorescein antibody (600101096; 0.2 μg/ml; Rockland Immunochemicals, PA), anti-mouse and human CHL1 antibody (AF2147 and MAB2126; R&D systems, MN; 1 μg/ml), HRP-conjugated anti-mouse and human CHL1 antibody (described above), anti-α2 integrin antibody (ab133557; Abcam; 1 μg/ml), anti-β1 integrin antibody (610467; BD transduction laboratories, NJ; 0.25 μg/ml), anti-FGFR3 antibody (c-15; Santa cruz, TX; 0.2 μg/ml 5% BSA-PBS), anti-TSG101 antibody (EXOAB-TSG101-1; System Biosciences, CA; 1:500), anti-CD63 antibody (EXOAB-CD63A-1; System Biosciences, CA; 1:500), anti-CD5L antibody (AF2834; R&D systems, MN; 0.4 μg/ml), anti-Pregnancy Zone Protein (PZP) antibody (PAG324Ra01; CLOUD-CLONE, TX; 0.5 μg/ml), anti-SLC4A1 antibody (18566-1-AP; PROTEINTECH, IL; 0.6 μg/ml), anti-Thrombospondin 1 (THBS1) antibody (PAA611Hu01; CLOUD-CLONE, TX; 0.5 μg/ml), and anti-caspase 14 antibody (MAB8215; R&D systems, MN; 0.5 μg/ml). The reaction with first antibody was carried out at room temperature for 1 hour to overnight. Then, the appropriate secondary antibody, HRP-conjugated anti-mouse IgG (Promega, WI; 1:3000-5000), HRP-conjugated anti-rabbit IgG (Promega, WI; 1:3000-5000), HRP-conjugated anti-goat IgG (Santa Cruz, TX; 1:3000-5000), Rabbit or Mouse TrueBlot®: anti-Rabbit or Mouse IgG HRP (Rockland Immunochemicals, PA; 1:1000), or HRP-conjugated anti-rat IgG (Santa Cruz; 1:3000-5000) were reacted at room temperature for 1 hour. After antibody treatment, the membranes were developed with an Immobilon Western Chemiluminescent HRP Substrate (Millipore, MA). The membrane was exposed and analyzed using ChemiDoc MP Image analyzer (BIO-RAD, CA). The molecular weight marker was a Pre-stained Protein Markers, Broad Range (Nacalai Tesque, Kyoto, Japan). For loading controls, SDS-PAGE gel was stained with Coomassie Brilliant Blue solution. In the case of membrane stripping, the membranes were treated with stripping solution (Wako Chemicals, Osaka, Japan) at room temperature for 20 min, re-blocking, and re-stained with appropriate antibody.

ELISA for CHL1 proteins in serum or EVs

The mouse serum CHL1 level was measured with direct ELISA method using HRP-conjugated anti-mouse and human CHL1 antibody as described previously (Kotani et al., 2018). In the case of the human CHL1 level in serum and serum EVs by sandwich ELISA, diluted serum or precipitated serum EVs described above were applied to the ELISA plates after coated with capture antibody, anti-human CHL1 antibody (10143-MM05; Sino Biological, Beijing, China), followed by the detection with HRP-conjugated anti-human CHL1 antibody (described above). The relative index (CHL1) for the measurement of mouse serum CHL1 levels were determined based on the value of standard sample described previously (Kotani et al., 2018). In human CHL1 ELISA, the recombinant human CHL1 partial protein (10143-H08H; Sino Biological, Beijing, China) was used as a standard.

ELISA for fluorescein-labeled proteins

For the sandwich ELISA to measure fluorescein-labeled SLC4A1 or caspase 14, 96 well ELISA plate (#3369; CORNING) was coated with anti-mouse and human SLC4A1 antibody (18566-1-AP; PROTEINTECH, IL; 1 µg/ml PBS) or anti-human caspase 14 antibody (H00023581-M01; Abnova, Taipei, Taiwan; 0.6 µg/ml PBS) at 4 °C for overnight. After blocking with 1% BSA-PBS (or 5% skim milk-PBS in caspase 14) solution at 37 °C for 1 hour, the corresponding EMARS products containing fluorescein-labeled SLC4A1 or fluorescein-labeled caspase 14 were added and incubated at 37 °C for 1 hour. Each well was washed gently with PBST (0.05 % tween-PBS solution), then treated with HRP-conjugated anti-fluorescein antibody (1 µg/ml), which was prepared from anti-fluorescein antibody *(*600101096; Rockland Immunochemicals, PA) using a peroxidase labeling kit NH_2 (Dojindo, Kumamoto, Japan) according to the manufacture's instruments, at 37 °C for 1 hour. In the case of the detection of SLC4A1 molecule itself, recombinant human SLC4A1 poly peptides (CSB-EP021663HU; CAUABIO THECHNOLOGY, Wuhan, China) and HRP-conjugated anti-SLC4A1 antibody, which was prepared using a Zenon rabbit IgG HRP Labeling Kit (Thermo Fisher Scientific, MA) according to the manufacturer's instrument, was used. The development was carried out with SureBlue/TMB Peroxidase Substrate (100 µl /each well; Sera care) at room temperature for appropriate minutes (3-10 min). After stopping the reaction using 2M HCl solution, the absorbance (O.D. 450 nm) was measured using Varioskan Flash microplate reader (Thermo Fisher Scientific, MA). The standard sample of fluorescein-labeled SLC4A1 (100 µl) was prepared as the EMARS products derived from 100 µl serum in large tumor-bearing *EML4-ALK* transgenic mouse (30 weeks old male). To compensate the differences among ELISA plates, the relative values were determined based on the value of standard sample as “BiEV index”. The “BiEV index (SLC4A1)” used in this study showed how many microliters corresponds to the above standard sample. In the case of fluorescein-labeled caspase 14, the “BiEV index (caspase 14)” was used based on the fluorescein-labeled recombinant

caspase 14 protein (11856-H07E; Sino Biological, Beijing, China) labeled with NHS-fluorescein (Thermo Fisher Scientific, MA). Caspase 14 protein (2.5 µg) and 8 µg NHS-fluorescein were mixed into 20 µl PBS, and then incubate at room temperature for 50 min. The reaction mixture was applied to mini column with approx. 0.5 ml Sephadex G-50 (GE Healthcare Life Sciences, IL) in order to remove excess NHS-fluorescein.

Statistical analysis

The statistical analyses and receiver operating characteristic (ROC) curve analysis for the data of ELISA measurement were performed using R software (The R Foundation for Statistical Computing, Austria) and EZR (Saitama Medical Center, Jichi Medical University, Japan) (Kanda, 2013), which is a graphical user interface for R. Statistical significance test of BiEV index of fluorescein-labeled SLC4A1 and caspase 14 between were performed with Mann–Whitney test. We used a statistical significance level of 0.05 or smaller. Similarly, the correlation between tumor mass and BiEV index (SLC4A1) was indicated using Spearman's rank correlation coefficient.

Results

Purification of serum EVs from *EML4-ALK* transgenic mice

A typical BiEV analysis of serum EVs is summarized in Figure 1. Western blot analysis of CD63 confirmed that EVs could be crudely purified from mouse serum by a polymer precipitation method (Figure 2A). CHL1, which is the molecule constituting LC BiCAT (Kotani et al., 2019), was also detected at higher levels in serum EVs from *EML4-ALK* transgenic mice (Supplementary Figure 1A). EMARS products from precipitated serum EVs (crude EVs) were detectable in CHL1 probe (+) samples, but not in EMARS probe (-) samples, indicating that EMARS reacts well with CHL1 probes and no serum factors induced non-specific EMARS reactions (Figure 2B). However, fluorescein-labeled EMARS products contained so many serum proteins (Data not shown) that size-exclusion chromatography was subsequently performed. The No. 6 to 8 fractions, fractionated by Sephacryl S-500 resin, were most suitable for collection of serum EVs with limited contamination of serum proteins (Figure 2C). The detection of TSG101 and ubiquitinated TSG101 (Jiao et al., 2009), a typical EV marker, supported a similar conclusion (Supplementary Figure 1B). Cryo-electron microscopy revealed many spherical particles measuring dozens of nanometers in size, with a lipid bilayer in fraction No. 6 to 8 samples (Figure. 2D), with each fraction containing EVs approximately 20–100 nm in diameter. No contamination with serum proteins seemed to be evident (Figure 2D). The EMARS products from purified serum EVs differed slightly depending on the S-500 fractions (Supplementary Figure 1C). In addition, the band patterns appeared to differ between samples with and without S-500 purification (Figure 2B and Supplementary Figure 1C).

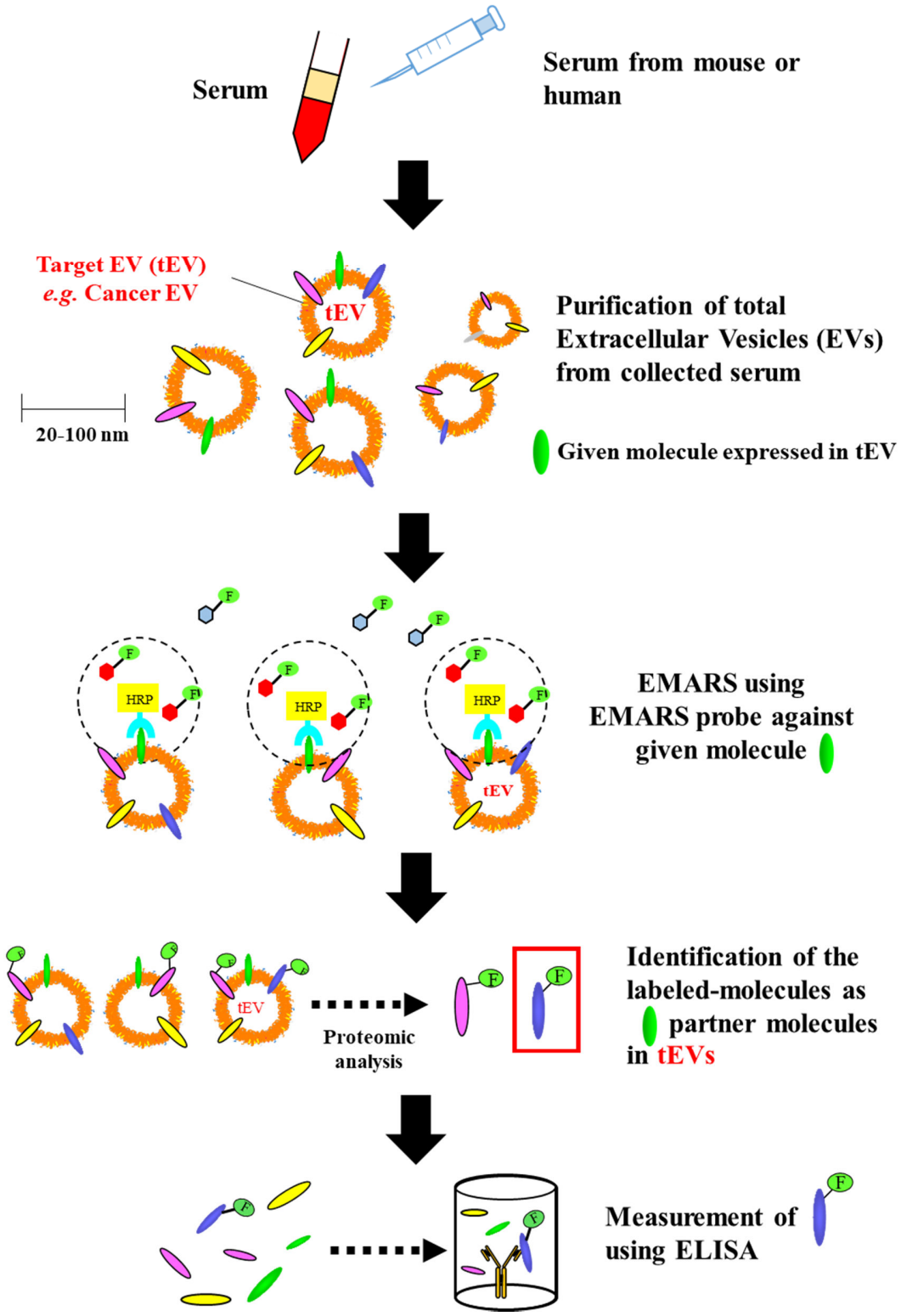

Figure 1 - Overview of BiEV analysis for serum EVs.
Schematic illustration of BiEV analysis for serum EVs. The target EV (tEV) indicates the EV to be detected and investigated. Before the EMARS reaction, serum EVs were purified using a combination of polymer-based precipitation and size-exclusion chromatography. To determine the amount of tEV in the sample by measuring the BiEV levels, appropriate BiEV partner molecules labeled with fluorescein were measured by a sandwich ELISA.

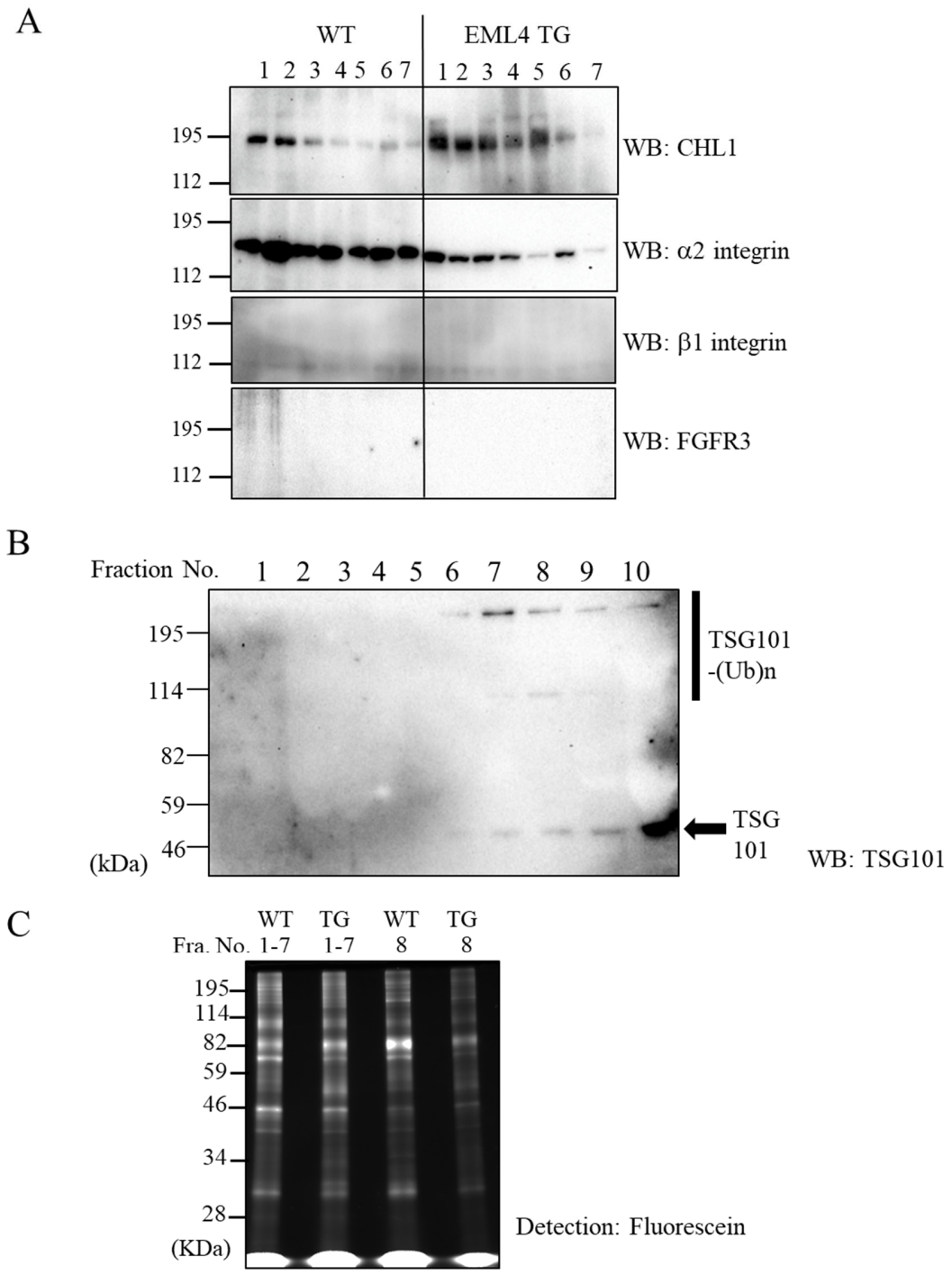

Supplementary Figure 1 - Characterization of crude and purified serum EVs
(*A*) Protein expression of precipitated EVs. The serum collected from seven mice of wild-type (WT) and *EML4-ALK* transgenic mouse (TL group) was subjected to Western blot analysis with anti-CHL1, anti-α2 integrin, anti-β1 integrin, and anti-FGFR3 antibodies, which were cancer cell membrane BiCAT molecules previously reported (8). (*B*) Western blot analysis for TSG101 antigen detection in Sephacryl S-500 fractions. The fractions were concentrated with *Nanosep*® centrifugal unit, and then subjected to Western blot analysis with anti-TSG101 antibody. TSG101-(Ub)n indicates ubiquitinated TSG101. (*C*) SDS-PAGE analysis of EMARS products in S-500 fraction. The fractionated EMARS products from serum EVs in wild-type and *EML4-ALK* transgenic mouse were subjected to SDS-PAGE analysis (10% gel) with fluorescence detection. The mixture of seven fractions (fraction No.1 to No. 7), and fraction 8 alone were respectively loaded in each well.

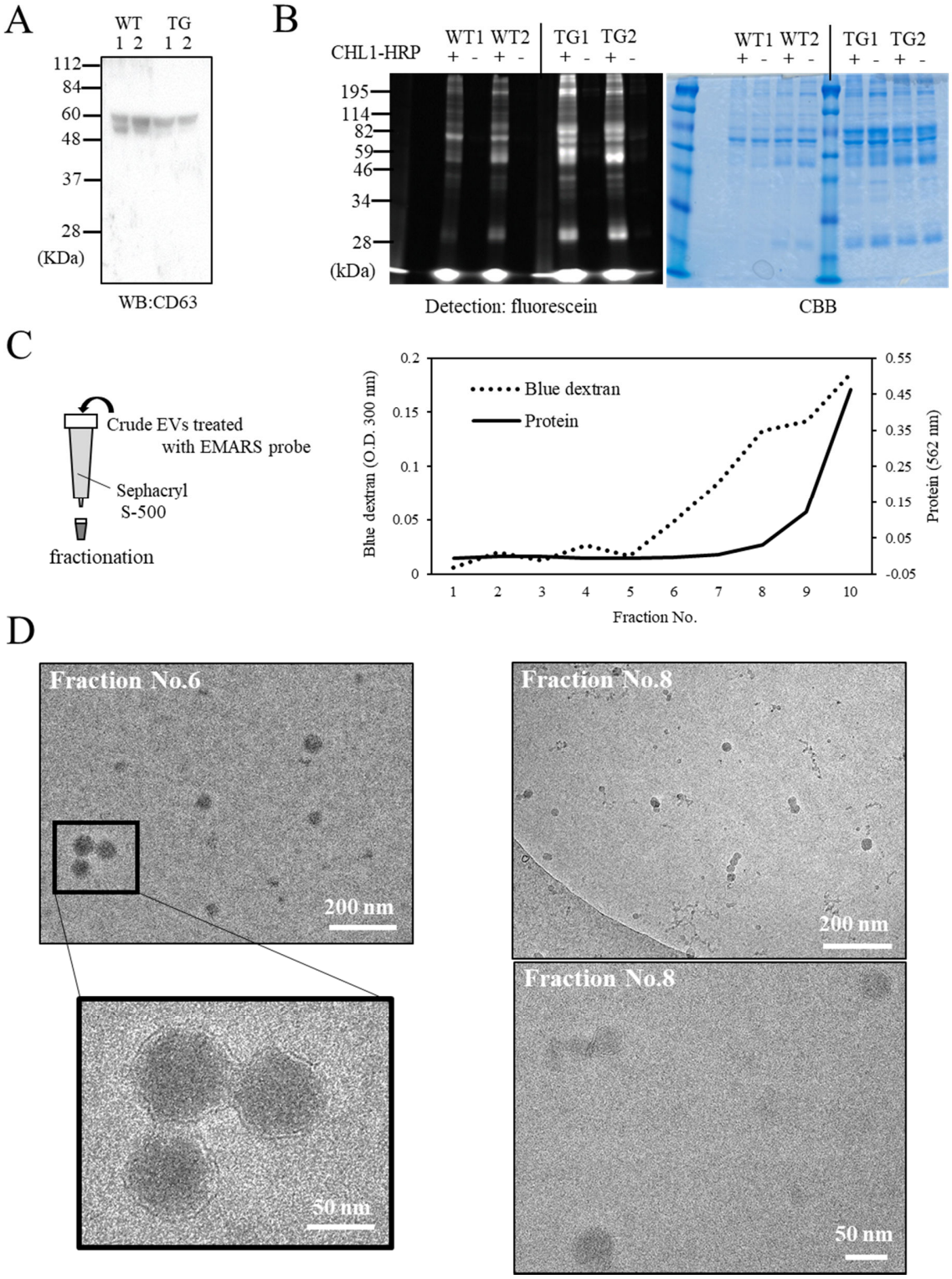

Figure. 2 – Purification of EVs from serum. (*A*) Western blot analysis of CD63 EV marker in precipitated EV samples. The precipitated EVs derived using ExoQuick Solution were prepared from the serum collected from 2 mice of wild-type (WT) and *EML4-ALK* transgenic (TG) mouse as described in the "*Materials and methods*". (*B*) Analysis of EMARS products obtained from EMARS reaction for crude mouse serum EVs. EMARS reaction was carried out directly in the precipitated serum EVs from two of WT and TG mice with or without HRP-conjugated CHL1 probe. The EMARS products were subsequently subjected to SDS-PAGE (10% gel) with fluorescein detection and CBB staining. (*C*) Fractionation using Sephacryl S-500 chromatography. Blue dextran (an indicator of void volume) and mouse serum (an indicator of protein elution) were used for preliminary experiments. The dotted line indicates absorbance of blue dextran. The solid line indicates protein concentration measured using a BCA protein kit. (*D*) Morphological observation of serum EVs (fraction No. 6 and No. 8) using cryo-electron microscopy. Lower panel of fraction No.6 is an enlarged view of a part of the upper panel. Scale bar; 200 nm (upper panel) and 50 nm (lower panel).

EMARS reactions for purified serum EVs from *EML4-ALK*transgenic mice

We first classified sera from three groups: wild-type (WT) mice, *EML4-ALK* transgenic mice with a large tumor (TL; tumor weight above 0.15 g), and *EML4-ALK* transgenic mice with a small tumor (TS; tumor weight 0.1 g or less). To obtain experimental results averaged over some mice, a 10 μL aliquot of the serum from 10 animals in each group was mixed in equal proportions, and then used for the following experiments. EMARS products were detected in the sample from TL mice in contrast to WT and TS mice (Figure 3A and 3B; "IP"). The band pattern of WT samples was similar to that of the TS sample (Figure 3A). TSG101 molecule was moderately abundant in the TL sample compared with the other two samples (Figure 3C), suggesting that the signals of EMARS products in the TL sample were due to a moderate increase in CHL1-expressed cEVs secreted from large tumor tissues. This supports the fact that fluorescein-labeled CHL1 molecules raised from self-labeling by EMARS with the CHL1 probe were abundant in TL (Figure 3D, upper panel; "IP"). In contrast, fluorescein-labeled α2 integrin in the TL sample was present at slightly lower levels than in the other two samples (Figure 3D, lower panel; "IP"). More CHL1-resident serum EVs were found in TL mice (Supplementary Figure 1A), but cEVs were not associated with an increase in CHL1-α2 integrin BiEV in contrast to BiCAT in LC cell membranes (Kotani et al., 2019). No critical differences in CHL1 levels on serum EV were found between WT and TS mice.

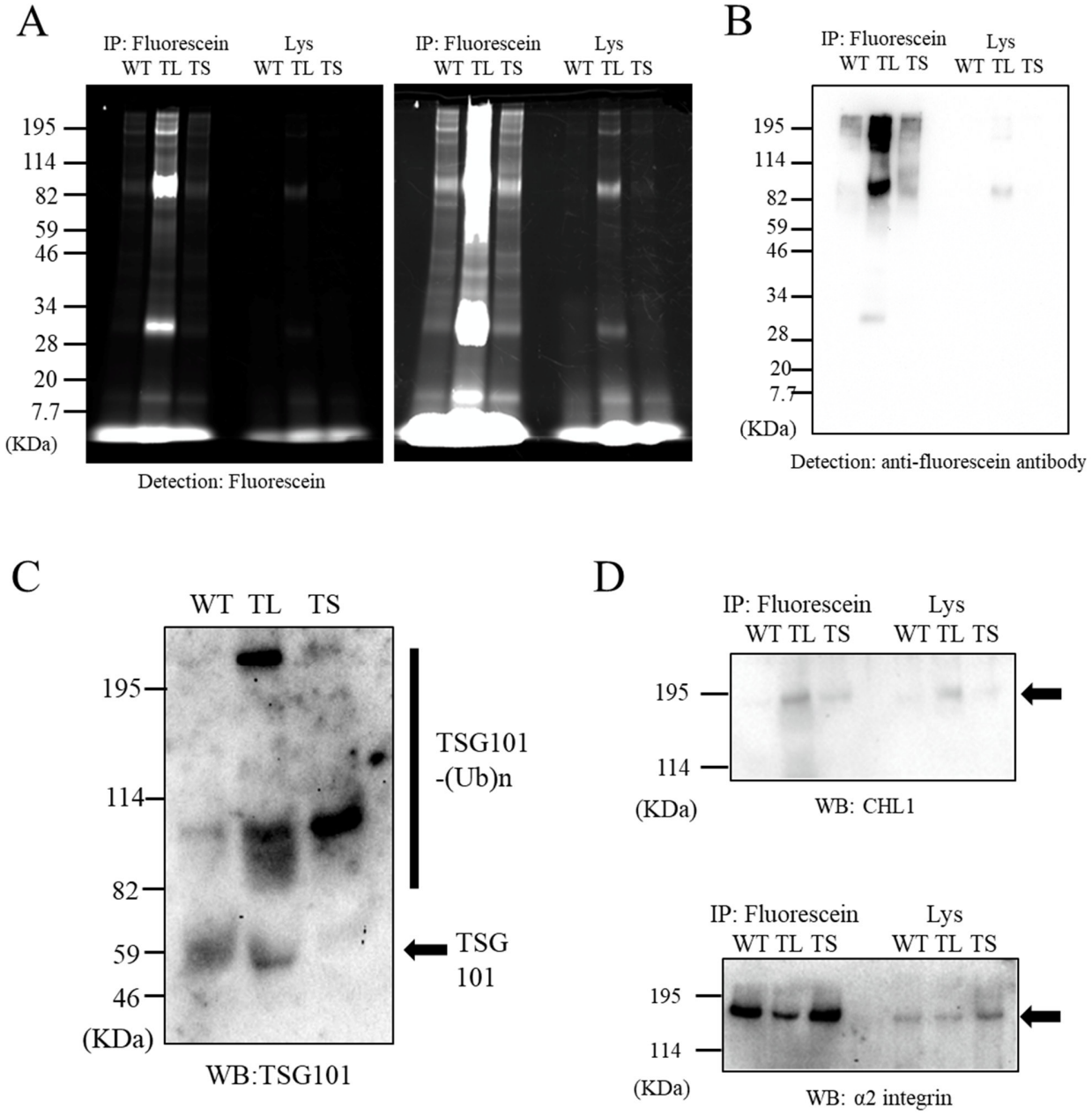

Figure 3 - BiEV analysis for serum EVs from *EML4-ALK* transgenic mouse.
(*A*) The EMARS products for serum EVs from *EML4-ALK* transgenic mouse. To average experimental results over each group, an aliquot of the serum (10 µL each) from 10 animals in each group (WT), large lung tumor-bearing (TL), and small lung tumor-bearing mice (TS) was mixed in equal proportions, and then applied to EV purification and EMARS. The EMARS products were concentrated and purified by immunoprecipitation with the anti-fluorescein antibody Sepharose. The resulting samples were subjected to SDS-PAGE analysis with fluorescence detection. "IP" indicates the immunoprecipitated samples, and "Lys" indicates the lysate samples before immunoprecipitation. The right panel indicates the same gel as the left panel, but exposed for a longer time. (*B*) Western blot analysis of fluorescein-labeled EMARS products from serum EVs using anti-fluorescein antibody. (*C*) Western blot analysis of TSG101 in serum EVs from WT, TL, and TS using anti-TSG101 antibody. Arrows indicate the detected band of monomer TSG101, and black bar indicates wide range of molecular weight due to an ubiquitination in TSG101 (TSG101-(Ub)n). (*D*) Western blot analysis of indicated samples with anti-CHL1 (upper panel) and anti-α2 integrin (lower panel) antibody. Arrow indicates the detected band of each molecule.

Identification of partner molecules of CHL1 in serum cEVs

In small tumor-bearing mice, specific BiEVs in serum cEVs may be difficult to detect due to the small amounts of labeled molecules. Candidates of BiEV partners of CHL1 suitable for small tumor screening in *EML4-ALK* transgenic mouse were examined by mass spectrometry (MS) proteomics, using both TL and TS EMARS products, as summarized in Table 1 (with raw data provided in Supplementary Table 1). We selected four candidate molecules (CD5L, PZP, THBS1, and SLC4A1). Western blot analysis using anti-CD5L antibodies revealed moderate bands at approximately 60 kDa in the TL samples, but no obvious bands were detected in the other two samples (Figure 4A; left panel). After stripping, the same membrane was re-stained with anti-PZP antibodies. PZP (approximately 130 kDa) was detected strongly in the WT sample (Figure 4A; right panel). The results indicate that some CHL1 BiEVs were also expressed in the serum EVs from WT mice. In contrast, western blot analysis using anti-SLC4A1 and anti-thrombospondin-1 (THBS1) antibodies revealed moderate bands in both TL and TS samples, but not in WT samples (Figure 4B). Similar dimer bands of SLC4A1 molecules were observed in an independent experiment (Figure 4C), which produced results identical to those shown in Figure 4B. In addition, we found that SLC4A1 and CHL1 molecules were expressed in LC tissue from *EML4-ALK* transgenic mice (Figure 4D and 4E). We therefore postulated that the measurement of CHL1-SLC4A1 BiEV in serum EVs may be an effective indicator for cEV screening in *EML4-ALK* transgenic mice.

Table 1. Candidates for the partners of CHL1 in serum EVs from WT, TL, and TS mice

Accession No.	Protein Name	Detected in
Q3UEI1	cAMP-specific 3',5'-cyclic phosphodiesterase 4C	WT
Q9QWK4	CD5 antigen-like (CD5L)	TL
P07724	Serum albumin	TL
Q61838	Pregnancy zone protein (PZP)	TL, TS
P02088	Hemoglobin subunit beta-1	TL
P08607	C4b-binding protein	TL
Q6Y4S4	Metastasis-suppressor KiSS-1	TL
Q8CDJ8	Stonin-1	TL
A1A535	Ventricular zone-expressed PH domain-containing protein 1	TL
Q91WK7	Ankyrin repeat domain-containing protein 54	TL
Q9JLM8	Serine/threonine-protein kinase DCLK1	TL
Q7SIG6	Arf-GAP with SH3 domain, ANK repeat and PH domain-containing protein 2	TL, TS
O88522	NF-kappa-B essential modulator	TL
Q9QWK5	Baculoviral IAP repeat-containing protein 1a	TL
Q6PFD7	Nuclear apoptosis-inducing factor 1	TL
P11276	Fibronectin	TL
P01942	Hemoglobin subunit alpha	TL
P35441	Thrombospondin-1 (THBS1)	TL, TS
P01029	Complement C4-B	TL, TS
Q8CDG3	Deubiquitinating protein VCIP135	TL
P01027	Complement C3	TL
Q8K0D7	Tail-anchored protein insertion receptor WRB	TL
Q9CQ26	STAM-binding protein	TL
O54990	Prominin-1	TL
Q8C3X4	Translation factor Guf1, mitochondrial	TL
Q8C4A5	Putative Polycomb group protein ASXL3	TL
Q5DTT3	Protein FAM208B	TL
Q62036	Centrosomal protein of 131 kDa	TL
P59530	Taste receptor type 2 member 7	TL
P04919	SLC4A1	TS
P60710	Actin, cytoplasmic 1	TS
P63101	14-3-3 protein zeta/delta	TS
P05213	Tubulin alpha-1B chain	TS
Q05816	Fatty acid-binding protein, epidermal	TS
O35173	Potassium voltage-gated channel subfamily S member 1	TS
Q925I1	ATPase family AAA domain-containing protein 3	TS

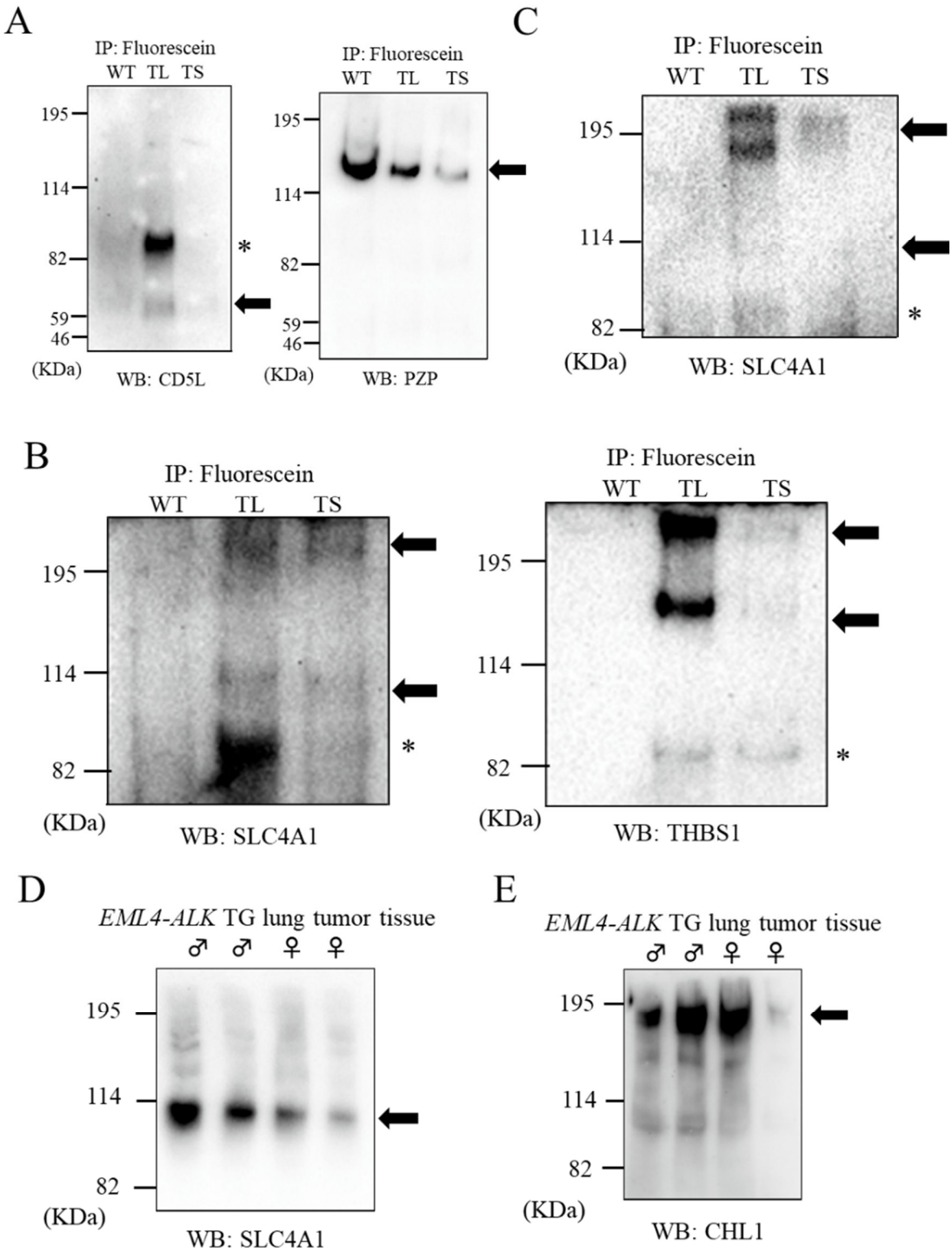

Figure 4 - Confirmation of partner molecules identified by MS proteomics.
(*A*) Confirmation of candidate partner molecules (CD5L and PZP) with mouse CHL1 in EVs. The EMARS products of WT, TL, and TS were respectively applied to immunoprecipitation (anti-fluorescence antibody Sepharose) and western blot analysis with anti-CD5L (left panel) antibody. After the stripping as described in the "*Materials and methods*", the membranes were re-stained with anti-PZP antibody (right panel). Arrows indicate the detected band of CD5L and PZP proteins (including predicted dimer). Asterisks indicate unknown bands (predicted as non-specific or partial fragments). (*B*) Confirmation of candidate partner molecules (SLC4A1 and THBS1) with mouse CHL1 in EVs. The western blot analysis was performed with anti-SLC4A1 antibody (upper panel). After stripping, the membranes were re-stained with anti-THBS1 antibody (lower panel). Arrows indicate the detected band of SLC4A1 and THBS1 proteins (including predicted dimers). Asterisks indicate unknown bands (predicted as non-specific or partial fragments). (*C*) Western blot analysis of an independent experiment samples identical to Figure 4B with anti-SLC4A1 antibody. Arrow indicates the detected band of predicted dimer SLC4A1 protein. Asterisk indicates unknown non-specific bands. (*D, E*) Expression of SLC4A1 (*D*) and CHL1 proteins (*E*) in tumor tissues from two male and two female *EML4-ALK* transgenic mice. The fragments of lung cancer tissues were mashed and washed gently with PBS, and then lysed with SDS-PAGE sample buffer directly. The resulting samples were subjected to Western blot analysis with anti-SLC4A1 antibody and anti-CHL1 antibody. Arrows indicate the detected band of monomer SLC4A1 and CHL1 proteins.

Measurement of CHL1-SLC4A1 BiEVs using a sandwich ELISA

The serum CHL1 level has been identified as a significant indicator of somewhat larger lung tumor-bearing *EML4-ALK* transgenic mice (Kotani et al., 2018). However, it was an insufficient indicator for small lung tumor-bearing *EML4-ALK* transgenic mice (Kotani et al., 2018). To determine whether the CHL1-SLC4A1 BiEV in serum EVs was elevated in *EML4-ALK* transgenic mouse, and TS mice in particular, measurement of fluorescein-labeled SLC4A1, which indicated an abundance of CHL1-SLC4A1 BiEV, was performed using a sandwich enzyme-linked immunosorbent assay (ELISA). Using recombinant SLC4A1 (partial protein) we determined that our ELISA could perform sensitive measurements of SLC4A1 (at least approx. 300 pg to 2000 pg/mL with linearity) as indicated by a correlation coefficient of 0.9995 in the calibration curve (Supplementary Figure 2A). However, fluorescein-labeled SLC4A1, which was made by a fluorescein-labeling reagent, did not perform well due to an unknown mechanism. We used EMARS products containing moderate amounts of fluorescein-labeled SLC4A1 obtained from one TL mouse serum EV as a standard. It was measured using horseradish peroxidase– conjugated anti-fluorescein antibodies (with a correlation coefficient of 0.995; Supplementary Figure 2B). To compare the results of each ELISA experiment in different plates, a BiEV index (SLC4A1) was based on the measured value of the standard substance (Supplementary Figure 2B).

The BiEV index (SLC4A1) from WT mice and *EML4-ALK* transgenic mice (detailed information for each is provided in Supplementary Table 2) is summarized in Figure 5A. Whereas CHL1 serum levels of small tumor-bearing mice were not significantly different from that of WT mice (Supplementary Figure 2C), the BiEV index (SLC4A1) in *EML4-ALK* transgenic mice had a tendency to be higher overall compared with WT mice (Figure 5A). The mean value of the BiEV index (SLC4A1) in WT mice was 0.1457 (standard deviation [SD] = 0.0679), and that in *EML4-ALK* transgenic mice was found to be 0.3162 (SD = 0.1979). The p value of 8.9×10^{-3} indicated a significant difference in CHL1-SLC4A1 BiEV levels between WT and *EML4-ALK* transgenic mice (Figure 5B). Based on the receiver operating characteristic (ROC) curve of each BiEV index (SLC4A1), the area under the curve (AUC) and cut-off value were calculated as 0.782 and 0.238, respectively (Figure 5C). In addition, a Spearman's rank correlation analysis indicated a slight correlation between the BiEV index (SLC4A1) and tumor mass (Figure 5D), suggesting that cEVs expressing CHL1-SLC4A1 BiEV were not secreted as much in the small tumor state, resulting in a moderate proportional correlation with tumor size. In contrast to increased CHL1-SLC4A1 BiEV in *EML4-ALK* transgenic mouse, a decrease in averaged SLC4A1 protein expression levels in whole-serum EVs was observed in *EML4-ALK* transgenic mice (Figure 5E).

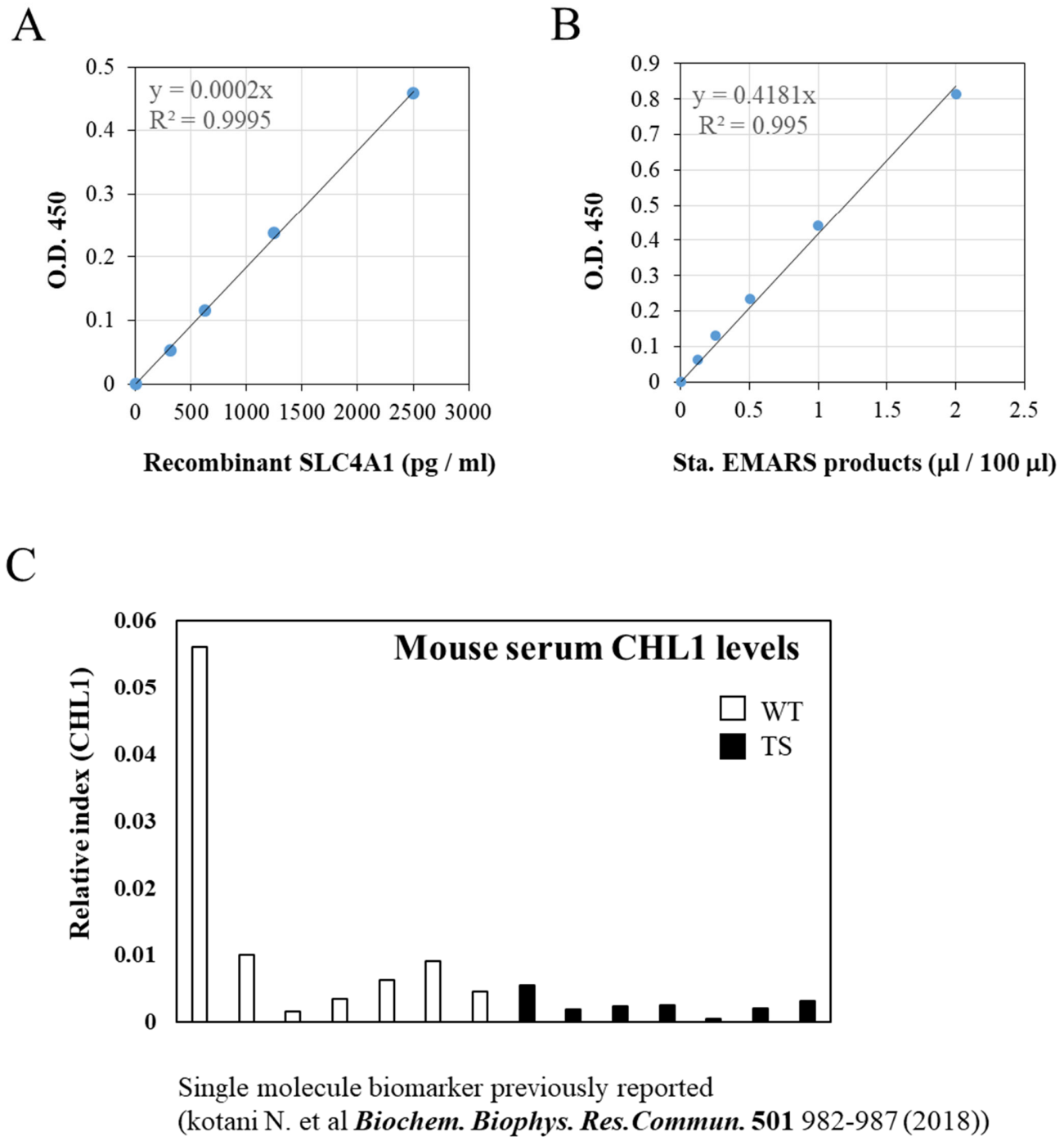

Supplementary Figure 2 - Characterization of ELISA system for SLC4A1
(*A, B*) Calibration curve of sandwich ELISA for the detection of both SLC4A1 partial proteins and fluorescein-labeled SLC4A1. The detection of several concentrations of recombinant SLC4A1 partial protein using HRP-labeled anti-SLC4A1 antibody which is prepared using Zenon system is summarized in (*A*). The detection of several concentrations of self-made standard materials containing fluorescein-labeled SLC4A1 using HRP-labeled anti-fluorescein antibody is summarized in (*B*). (*C*) Comparison of serum CHL1 levels between wild-type (WT) and small tumor-bearing *EML4-ALK* transgenic (TS) mice by using previously established ELISA system for CHL1 measurement. There were no significant differences between them.

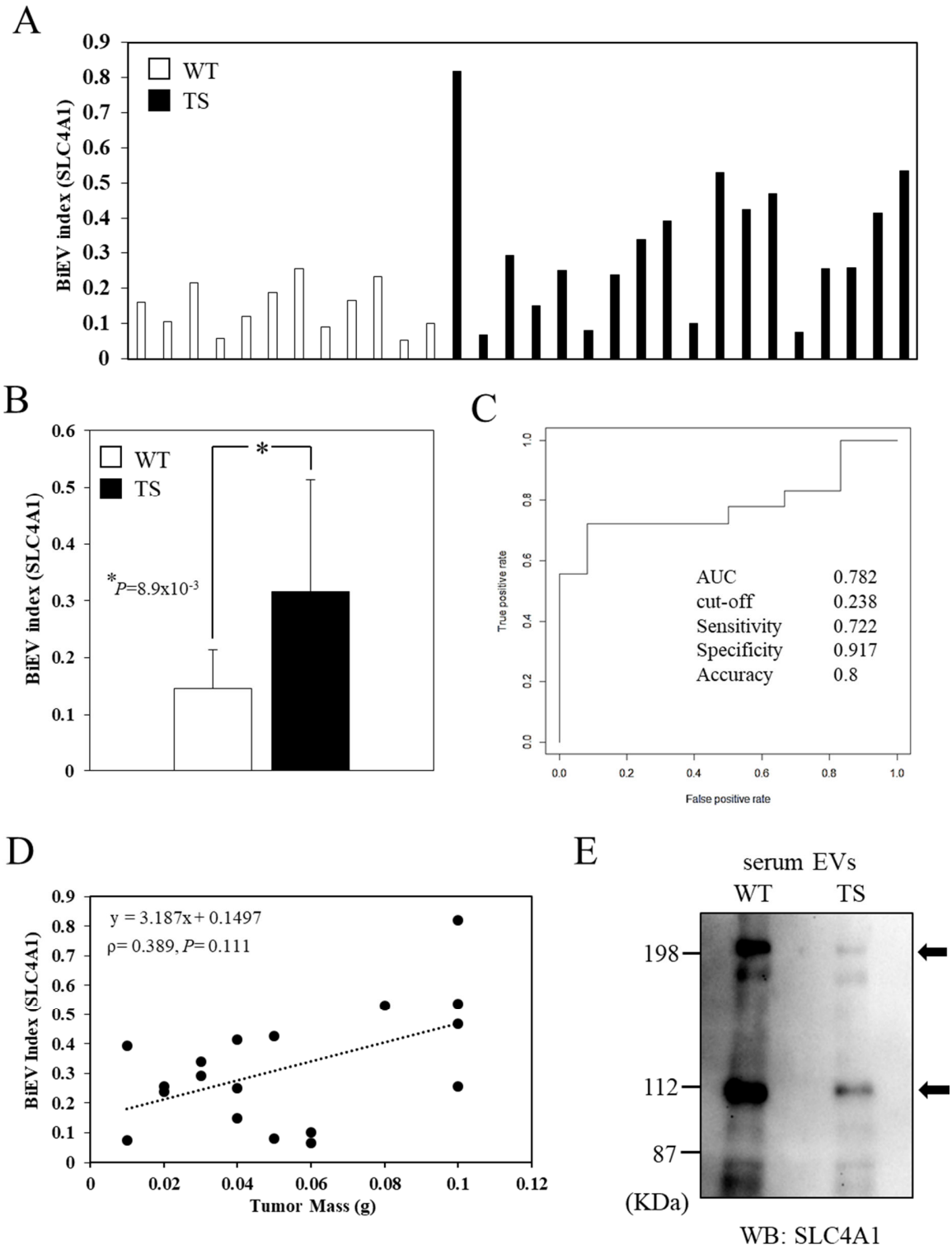

Figure 5 - Measurement of CHL1-SLC4A1 BiEV in serum EVs. (*A*) Measurement of fluorescein-labeled SLC4A1 using a sandwich ELISA. The serum EVs from 12 wild-type mice (open bar) and 18 small lung tumor-bearing *EML4-ALK* transgenic mice (closed bar) were applied to EMARS reactions followed by ELISA measurements, respectively. The EMARS products containing fluorescein-labeled SLC4A1 were added to anti-SLC4A1 antibody-coated ELISA plates. A BiEV index (SLC4A1) was calculated based on the value of fluorescein-labeled SLC4A1 in standard samples. (*B*) Comparison of BiEV indexes between WT and TS. The BiEV indexes of TS were significantly higher than that of WT ($p = 8.9 \times 10^{-3}$) by a Mann–Whitney test. (*C*) ROC curve for BiEV indexes. AUC was calculated as 0.782. (*D*) A scatter-plot of tumor mass versus BiEV index. Correlation between BiEV index and lung tumor mass of TS was estimated using Spearman's rank correlation coefficient (0.389: $p = 0.111$). (*E*) Western blot analysis of SLC4A1 in whole-serum EVs from WT and TS. An aliquot of the serum from 12 animals in the wild-type group and 18 animals in small lung tumor-bearing *EML4-ALK* transgenic mice was mixed in equal proportions followed by EV purification. Arrows indicate the detected band of SLC4A1. Asterisks indicate unknown bands (predicted as non-specific or partial fragments).

BiEV analysis and measurement in lung cancer patients

Because BiEV was found to be useful for screening serum EV in mice, a similar analysis was performed using serum EVs from healthy person (H) and LC patients. To examine whether CHL1 alone is a significant difference between H and LC patients, CHL1 levels of serum and serum EV were measured by ELISA (a correlation coefficient of 0.9878 in a calibration curve: Supplementary Figure 3A) using a previously described technique (Kotani et al., 2018). No significant differences between H and LC were found (Figure 6A and 6B), suggesting that BiEV analysis was needed as well as model mouse.

As with the model mouse experiments, an aliquot of the serum from healthy person and LC patients (detailed information is provided in Supplementary Table 3) was mixed in equal proportions, and then used for the following experiments. EMARS products using CHL1 EMARS probe were detected in both serum EVs, although the band pattern of the H samples was similar to that of LC samples, as with the WT and TS mice (Figure 6C). To determine whether fluorescein-labeled SLC4A1 as identified in the model mouse experiments could be detected in human LC samples, EMARS products from H and LC were subjected to SLC4A1 western blot analysis and ELISA quantification. No crucial differences between H and LC (Figure 6D and 6E) were seen, indicating that identification of more suitable BiEV should be needed in the human samples. The candidates of BiEV partners of human CHL1 were identified by MS proteomics (summarized in Table 2, with raw data provided in Supplementary Table 4 and a summary of mass scores in Supplementary Table 5). Immunoprecipitation and western blot analysis revealed that caspase 14, which is family member of caspase involved in keratinocyte differentiation (Denecker et al., 2008), was detected at significant levels as a partner of CHL1 BiEV in serum EVs from LC (Figure 7A) (Mikolajczyk et al., 2004; Van de Craen et al., 1998). Fluorescein-labeled caspase 14 was also detected in EMARS products of secreted EVs from LK2 culture cells (Table 2), suggesting that CHL1–caspase 14 BiEV is a typical indicator of cEV in LC. We therefore postulated that the measurement of CHL1–caspase 14 BiEV in serum EVs is a suitable indicator for the cEV screening in LC.

To measure fluorescein-labeled caspase 14 in EMARS products using sandwich ELISA, a fluorescein-labeled caspase 14 standard was prepared using recombinant caspase 14. The caspase 14 ELISA system was suitable for sensitive measurement of the fluorescein-labeled caspase 14 standard with a correlation coefficient of 0.9878 in a calibration curve (Supplementary Figure 3B). To compare the results among each ELISA experiment in different plates, a BiEV index (caspase 14) was set based on the measured value (ng/mL) of the fluorescein-labeled caspase 14 standard.

The BiEV index (caspase 14) from the H and LC serum EVs is summarized in Figure 7B. LC EVs had a tendency to be higher overall than that in H EVs. The mean value of the BiEV index (caspase 14) in H EVs was 1.065 (SD = 1.168), and that in LC EVs was 3.707 (SD = 2.829). A p value of 0.019 indicated a significant difference in CHL1–caspase 14 BiEV levels between the H and LC EVs (Figure 7C). Based on the ROC curve

of each BiEV index, the calculated AUC and cut-off value were 0.811 and 1.889, respectively (Figure 7D). No increase in total protein expression levels of caspase 14 molecules in whole-serum EVs between H and LC serum EVs was found (Figure. 7E).

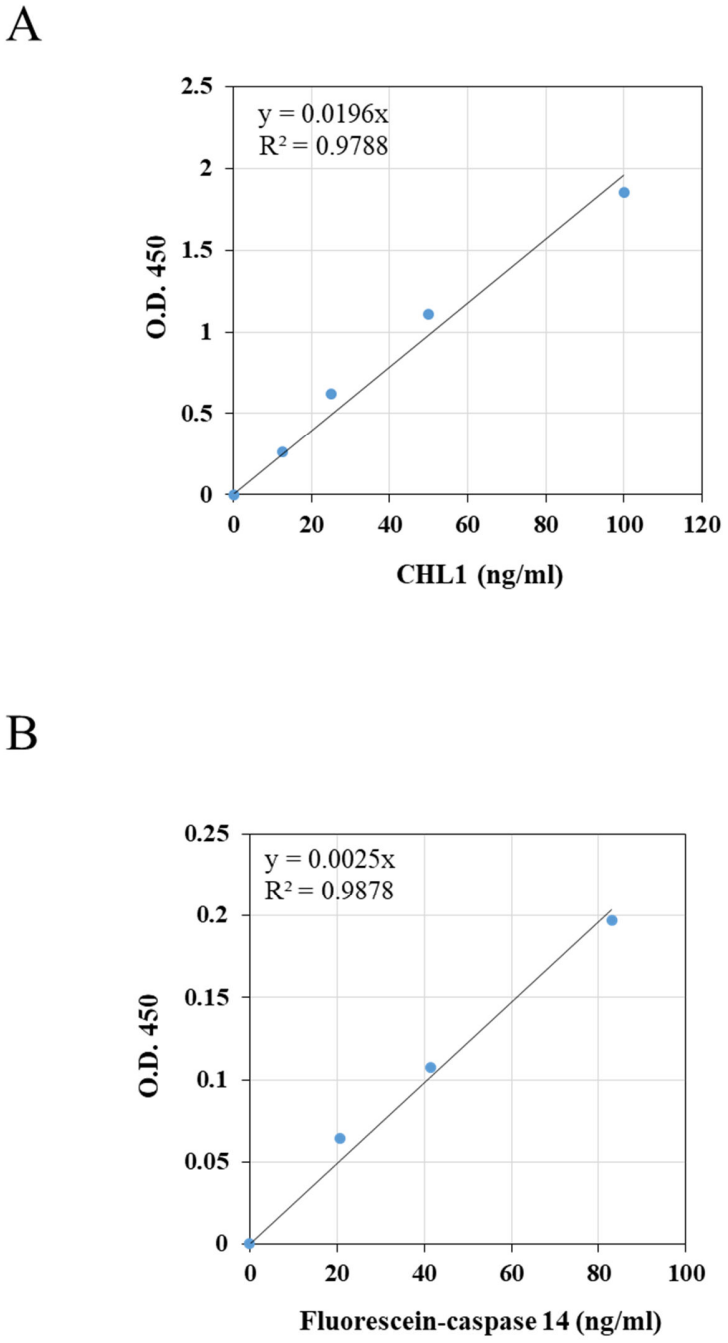

Supplementary Figure 3 - Characterization of ELISA system for fluorescein labeled-caspase 14 and human CHL1

(*A, B*) Calibration curve of sandwich ELISA for the detection of both human CHL1 and fluorescein-labeled caspase 14. The detection of several concentrations of recombinant human CHL1 partial protein using HRP-labeled anti-CHL1 antibody is summarized in (*A*). The detection of several concentrations of fluorescein-labeled caspase 14 standard using HRP-labeled anti-fluorescein antibody is summarized in (*B*).

Figure 6 - Measurement of CHL1-SLC4A1 BiEV in serum EVs from lung cancer patients

(*A*) Comparison of serum CHL1 levels between H (open bar) and LC (closed bar) by using ELISA system for human CHL1 measurement. There were no significant differences between them. (*B*) Comparison of serum EV CHL1 levels between H (open bar) and LC (closed bar) by using ELISA system. There were also no significant differences between them. (*C*) EMARS products purified from serum EVs of healthy person (H) and lung cancer (LC) patients. Fifty microliters of mouse serums was collected from the H and LC groups, and utilized in EV purification followed by EMARS reactions. To average experimental results over each group, an aliquot of the serum (10 µL each) from 5 H and 5 LC was mixed each in equal proportions. The EMARS products were subjected to SDS-PAGE analysis with fluorescence detection. (*D*) Confirmation of human CHL1-SLC4A1 BiEV in serum EVs. The healthy person (H) and lung cancer patients (LC) EAMRS samples were respectively applied to immunoprecipitation (anti-fluorescence antibody Sepharose) and western blot analysis with anti-SLC4A1 antibody. Arrows indicate the detected band of human SLC4A1 proteins (including predicted dimer). (*E*) Measurement of fluorescein-labeled human SLC4A1 using sandwich ELISA system used in mouse fluorescein-labeled SLC4A1. The serum EVs from 6 H (open bar) and 6 LC (closed bar) were applied to EMARS reaction followed by ELISA measurement, respectively. The EMARS products containing fluorescein-labeled SLC4A1 were added to anti-SLC4A1 antibody-coated ELISA plates. "BiEV index (SLC4A1)" was calculated based on the value of fluorescein-labeled SLC4A1 in standard samples as described in "*Materials and methods*".

Table 2 Candidates for the partners of CHL1 in serum EVs from lung cancer patients

Accession No.	Protein Name	Also detected in LK2 EVs*
P15924	Desmoplakin	○
P02788	Lactotransferrin	○
P31947	14-3-3 protein sigma	○
P04792	Heat shock protein beta-1	
P07355	Annexin A2	○
P27482	Calmodulin-like protein 3	
P47929	Galectin-7	○
Q08554	Desmocollin-1	○
Q01469	Fatty acid-binding protein 5	○
P37802	Transgelin-2	
P04083	Annexin A1	○
P06733	Alpha-enolase	
P09211	Glutathione S-transferase P	
Q13885	Tubulin beta-2A chain	
P63104	14-3-3 protein zeta/delta	○
P31944	Caspase-14	○
P68366	Tubulin alpha-4A chain	
P58107	Epiplakin	
P01833	Polymeric immunoglobulin receptor	○
P68363	Tubulin alpha-1B chain	
P29508	Serpin B3	○
P68371	Tubulin beta-4B chain	
P60174	Triosephosphate isomerase	
Q9HCY8	Protein S100-A14	
P31949	Protein S100-A11	○
Q96DA0	Zymogen granule protein 16 homolog B	○
Q9NZT1	Calmodulin-like protein 5	
P02545	Prelamin-A/C	
P68104	Elongation factor 1-alpha 1	○
P11142	Heat shock cognate 71 kDa protein	○

* “LK2 EVs” were purified from the culture supernatant of LK2 lung cancer cell line which expresses CHL1.

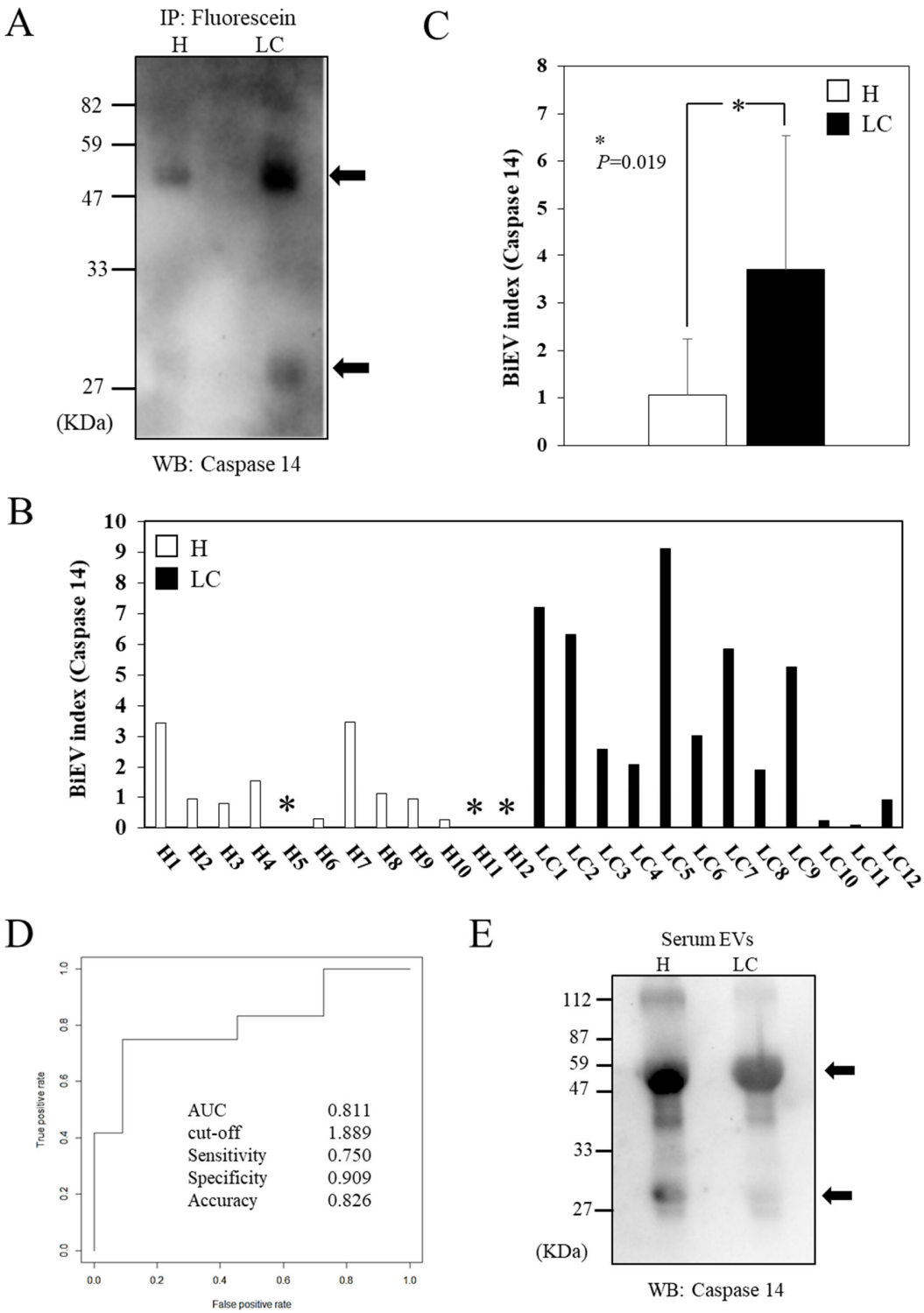

Figure 7 - Measurement of CHL1-caspase 14 BiEV in serum EVs from lung cancer patients.
(*A*) Confirmation of partner molecules with CHL1 identified by MS proteomics. The H and LC samples were applied respectively to immunoprecipitation (anti-fluorescence antibody Sepharose) and western blot analysis with anti-caspase 14 antibodies. Arrows indicate the detected band of caspase 14 proteins (including predicted dimer). (*B*) Measurement of fluorescein-labeled caspase 14 using a sandwich ELISA. Serum EVs from 12 H (open bar) and 12 LC (closed bar) were applied to EMARS reactions followed by ELISA measurements, respectively. The EMARS products containing fluorescein-labeled caspase 14 were added to anti-caspase 14 antibody-coated ELISA plates. "BiEV index (caspase 14)" was calculated based on the value of fluorescein-labeled recombinant caspase 14 made by fluorescein-labeling regent. The values are shown as the average of three independent ELISA experiments using the same samples. The detail data of H and LC persons is provided in Supplementary Table 3. Asterisks indicate the samples were below detection limit. (*C*) Comparison of BiEV indexes between H and LC. The BiEV indexes of LC were significantly higher than that of H ($p = 0.019$) by a Mann–Whitney test. (*D*) ROC curve for BiEV indexes. The AUC was calculated as 0.811. (*E*) Western blot analysis of caspase 14 in whole-serum EVs from H and LC. An aliquot of the serum (2 μL each) from 12 persons in H and LC was mixed in equal proportions followed by EV purification with precipitation protocol. Arrows indicate the detected band of caspase 14.

Discussion

Taking into consideration the potential and expectation for bimolecular strategies identified by previous studies, we examine the possibility of applying BiEV to EV screening and clinical applications. Because several functional EVs, including exosomes, have been investigated as potential secretable biomarkers for precision medicine (Colombo et al., 2014). We focused on a characterization of serum EVs as a BiEV carrier to develop a new strategy for EV screening. It was once assumed that partner molecules of CHL1 in cell membranes and EVs were similar because EVs may contain BiCATs (Kotani et al., 2019), which exist in cancer cell membranes as BiEVs. Despite the presence of three BiCATs in transport vesicles, as confirmed by electron microscopy (Kotani et al., 2019), this was not the case with BiCATs in serum cEV (Supplementary Figure 1A). This likely because the transport vesicles described in the BiCAT report were not involved in EV formation, or the membrane components constituting EVs in *EML4-ALK* transgenic mouse were originally different or altered cancer cell membranes.

We chose to independently examine BiEVs in serum cEV using EMARS. In an analysis of serum EVs, purification of serum EVs (Figure 2C) was an important sequence, because EMARS reactions labeled many serum proteins utilizing insufficient purification samples (Baranyai et al., 2015; Schey et al., 2015). Although several purification methods are available for EVs, we selected size-exclusion chromatography (de Menezes-Neto et al., 2015) because of its simplicity of handling and low costs. Our gel-purification system was useful for collecting and purifying many EV particles without serum proteins. However, in purified EVs, some soluble serum proteins were detected by the EMARS reaction. These serum proteins may be adsorbed by the EV itself in the bloodstream and/or in the EV secretion pathway from cancer cell and may be present in the proximity of CHL1. Whether these are simply adsorbed or have the property of adsorbing specifically to EV surface molecules is unknown.

A previous study has shown that CHL1 expression in serum EVs was increased in large tumor-bearing mice (Kotani et al., 2018), and in this study, CHL1 BiEV was greatly increased in large tumor-bearing mice (Figure 3). This is the result of upregulated secretions of EVs expressing CHL1, increased expression of CHL1 on EVs, or both. In any case, purified and detected EVs were considered to contain EVs secreted from *EML4-ALK* LC cells. CHL1 BiEV can therefore be used as an indicator of cEV, but confirmation is needed. The candidate partner molecules for CHL1 BiEV in Table 1 have been identified by MS, and another confirmation technique, such as immunoprecipitation or western blot experiments, is required to identify whether they are true partner molecules. Among the molecules listed in Table 1, some candidates BiEV partner molecules did not form BiEVs specifically in serum EVs from LC (Figure 4A). In contrast, CHL1-THBS1 and CHL1-SLC4A1 BiEV were clearly expressed in serum EV even in LC model mice, particularly in individuals with small tumors (Figure 4B).

In this study, we preferentially analyzed SLC4A1, a membrane protein, and compared it with THBS1. However, because several studies have reported THBS1 is expressed in exosomes and is also involved in cancer cell migration, invasion, metastasis, and epithelial-mesenchymal transition, further study is warranted (Cen et al., 2019; Huang et al., 2019; Tauro et al., 2013).

ELISA quantification revealed that the CHL1-SLC4A1 BiEV in mouse serum EVs are applicable biomarkers for screening small tumors in *EML4-ALK* transgenic mice (Figure 4 and 5) compared with the serum CHL1 level, which is a single biomarker for LC cells, as reported previously (Kotani et al., 2018). Tumor size in *EML4-ALK* transgenic mouse was partially correlated with the value of CHL1-SLC4A1 BiEV (Figure 5D) supporting the evidence for direct secretion of such EVs in cancer cells. These advantages allowed us to discuss not only the sensitivity of BiEV analysis for typical EV screening but also its applicability to cancer screening in human cancer patients, who usually present with small tumor masses. The SLC4A1 molecule is a multi-pass transmembrane chloride bicarbonate exchange transporter (Reithmeier et al., 2016). In addition, it has also been found to be markedly upregulated in several cancer cells (Gorbatenko et al., 2014). However, the average expression level of SLC4A1 in the whole-serum EVs was lower in LC model mice that in WT mice (Figure 5E). The amount of fluorescein-labeled SLC4A1, which is indicated as CHL1-SLC4A1 BiEV, should be quantified using this BiEV analysis.

The application of BiEV analysis in human serum EV screening is an important issue. According to our study, CHL1-SLC4A1 BiEV detected in mouse LC did not appear to be significant in human LC patients (Figure 6D and 6E). It is therefore necessary to identify the appropriate BiEV according to animal species as well as cancer type. In human screening, it is assumed that the appropriate BiEV differs by tissue type within a cancer type. In the case of LC, small cell carcinoma, non-small cell carcinoma, adenocarcinoma, and squamous cell carcinoma, among others, are listed as categories. In consideration of experimental efficiency and the value of human serum sources, our experiments were performed by integrating serum, but it will be important to study these factors in the future.

In this study, we have shown that measurement of CHL1–caspase 14 BiEV may be useful for screening cEV in LC patients. Interestingly, CHL1–caspase 14 BiEV has also been detected in EVs secreted from LK2 human LC cells with serum-free medium (Table 2), suggesting that EVs expressing CHL1–caspase 14 BiEV were directly secreted from LC cells. Unlike SLC4A1, Caspase 14 is a caspase family protease (Van de Craen et al., 1998), not a membrane protein, whose subcellular localization is said to be in the nucleus and cytoplasm (Alibardi et al., 2004). Although there has been no obvious evidence of the presence of caspase 14 in serum, it is possible that caspase 14 was adsorbed to EV in blood stream. However, LK2 cell secretion experiments with serum-free medium concluded that serum EV with CHL1–caspase 14 BiEV targeted in this study may display caspase 14 on the EV surface during the process of EV formation in LC cells. Similar to SLC4A1 in mice, the high expression levels of caspase 14 itself has been observed in cancer cells (Fang et al., 2011; Koenig et al.,

2005; Krajewska et al., 2005), but expression of caspase 14 in healthy EVs and cancer EVs exhibited no significant differences as a whole (Figure 7E). This also demonstrates that fluorescein-labeled caspase 14 should be quantified in BiEV analysis.

BiEV strategies have some problems to overcome. Although the cause is unknown, in some cases, neither CHL1-SLC4A1 nor CHL1–caspase 14 BiEV were increased in serum EVs even in *EML4-ALK* transgenic mouse and LC (Figure 5 and 7). Because cancer screening does not perform multiple tests of biomarkers, it is necessary to search for appropriate BiEVs to produce high AUC scores in ROC analyses (Figure 5C and 7D). In addition, serum EV purification and EMARS reactions of the BiEV strategy were slightly complicated and time consuming. As a solution, a novel ELISA technique is required. Because serum EVs were approximately 20 to 100 nm in size according to cryo-electron microscopy (Figure 2D), a more reasonable fluorescein-labeling distance (within 20 nm (Kotani et al., 2019)) would allow a BiEV to be measured directly by the ExoScreen method, which easily detects and quantifies proximal molecules in an EV particle (Yoshioka et al., 2014). To use BiEV information in the clinical field, development of such a system will be necessary.

Taken together, the BiEV strategy proved useful for the screening in EV classification. Considerable advantages should become apparent if these BiEVs are used as a novel biomarker (cancer EV antigen) for cancer screening or at least molecular diagnosis (Supplementary Figure 4).

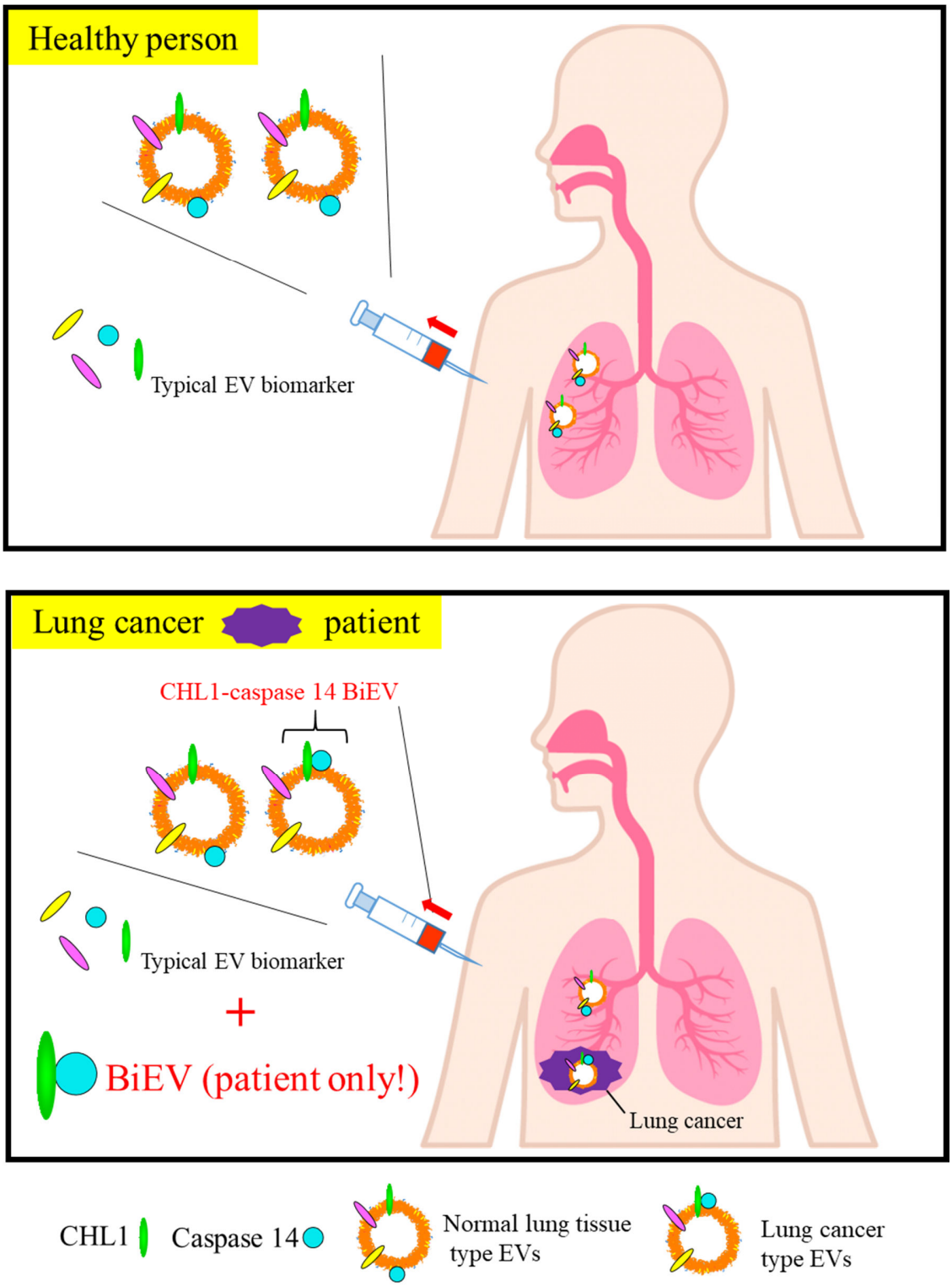

Supplementary Figure 4 - Summary of advantages for human EV screening using BiEV
One of hypothetical mechanisms of BiEV differences between human healthy and lung cancer patients is summarized in this figure based on our results of no significant differences of CHL1 and caspase 14 expression levels. Due to the hypothetical mechanisms, it is considerable that our BiEV analysis is useful when it is difficult to characterize secreted cancer EVs by single molecular index (*e.g.* serum CHL1 single screening and typical serum biomarker (CEA and SCC in Supplementary Table 3)). In this study, BiEV analysis may emphasize the differences using the information of bimolecular complex which is formed by association between CHL1 and caspase 14 with unknown cancer cell-specific mechanisms.

Acknowledgments

We thank Professor Hiroyuki Mano and Dr. Manabu Soda for providing *EML4-ALK* transgenic mice; Medical Genome Center Biobank, National Center for Geriatrics and Gerontology and BioBank Japan Project (supported by AMED) for providing human serum samples; Laboratory of Cytometry and Proteome Research, Tokyo Medical and Dental University, and Ms. Amimoto of the Natural Science Center for Basic Research and Development (N-BARD), Hiroshima University for MS technical assistance; Professor Tsumoru Shintake for helping with electron microscopic analysis; Kochi University's experimental training equipment facility and the Saitama Medical University Biomedical Research Center for providing general technical assistance. This work was supported by Grants-in-aid for Scientific Research in Japan (No. JP15K07941, and No. JP18K06663 to N. K.; JP17H04409 to T. S.), Mizutani foundation research grants (to N. K.), and Japan science and technology grants (to N. K.). We also thank enago group for editing a draft of this manuscript.

Abbreviations

EV; extracellular vesicle, cEV; cancer cell-secreted EV, tEV; cEV; target EV, BiEV; bimolecular surface antigen expressed in EV, EMARS; enzyme-mediated activation of radical source, BiCAT; Bimolecular Cancer Target, CHL1; close homolog of L1, LC; lung cancer, MS; mass spectrometry.

Authors' Contributions

Conceptualization, N.K.; Methodology, N.K., H.K., R.K., and T.N.; Investigation, N.K., H.K., R.K., Y.I., I.S.; Resources, H.T. and T.S., T.M., and K.H.; Data Curation, N.K.; Writing-Original Draft, N.K.; Writing - Review & Editing, H.K., R.K., T.N., T.S., T.M., K.H. and N.K.; Supervision, N.K., and K.H.; Funding Acquisition, N.K. T.S., and K.H.

Potential Conflict of Interest

The authors declare that they have no conflicts of interest with the contents of this article.

References

Alibardi L, Dockal M, Reinisch C, Tschachler E, Eckhart L. 2004. Ultrastructural localization of caspase-14 in human epidermis. *J Histochem Cytochem* **52**:1561–74. doi:10.1369/jhc.4A6300.2004

Anfossi S, Babayan A, Pantel K, Calin GA. 2018. Clinical utility of circulating non-coding RNAs — an update. *Nat Rev Clin Oncol* **15**:541–563. doi:10.1038/s41571-018-0035-x

Baranyai T, Herczeg K, Onódi Z, Voszka I, Módos K, Marton N, Nagy G, Mäger I, Wood MJ, El Andaloussi S, Pálinkás Z, Kumar V, Nagy P, Kittel Á, Buzás EI, Ferdinandy P, Giricz Z. 2015. Isolation of Exosomes from Blood Plasma: Qualitative and Quantitative Comparison of Ultracentrifugation and Size Exclusion Chromatography Methods. *PLoS One* **10**:e0145686. doi:10.1371/journal.pone.0145686

Brown DA, London E. 1998. FUNCTIONS OF LIPID RAFTS IN BIOLOGICAL MEMBRANES. *Annu Rev Cell Dev Biol* **14**:111–136. doi:10.1146/annurev.cellbio.14.1.111

Cen J, Feng L, Ke H, Bao L, Li LZ, Tanaka Y, Weng J, Su L. 2019. Exosomal Thrombospondin-1 Disrupts the Integrity of Endothelial Intercellular Junctions to Facilitate Breast Cancer Cell Metastasis. *Cancers (Basel)* **11**:1946. doi:10.3390/cancers11121946

Cocucci E, Meldolesi J. 2015. Ectosomes and exosomes: shedding the confusion between extracellular vesicles. *Trends Cell Biol* **25**:364–372. doi:10.1016/j.tcb.2015.01.004

Colombo M, Raposo G, Théry C. 2014. Biogenesis, Secretion, and Intercellular Interactions of Exosomes and Other Extracellular Vesicles. *Annu Rev Cell Dev Biol* **30**:255–289. doi:10.1146/annurev-cellbio-101512-122326

de Menezes-Neto A, Sáez MJF, Lozano-Ramos I, Segui-Barber J, Martin-Jaular L, Ullate JME, Fernandez-Becerra C, Borrás FE, Del Portillo HA. 2015. Size-exclusion chromatography as a stand-alone methodology identifies novel markers in mass spectrometry analyses of plasma-derived vesicles from healthy individuals. *J Extracell vesicles* **4**:27378.

Denecker G, Ovaere P, Vandenabeele P, Declercq W. 2008. Caspase-14 reveals its secrets. *J Cell Biol* **180**:451–8. doi:10.1083/jcb.200709098

Fang H-Y, Chen C-Y, Hung M-F, Hsiao Y-T, Chiang T-C, Lin T-Y, Chang H-W, Chow K-C, Ko W-J. 2011. Caspase-14 is an anti-apoptotic protein targeting apoptosis-inducing factor in lung adenocarcinomas. *Oncol Rep* **26**:359–69. doi:10.3892/or.2011.1292

Gorbatenko A, Olesen CW, Boedtkjer E, Pedersen SF. 2014. Regulation and roles of bicarbonate transporters in cancer. *Front Physiol* **5**:130. doi:10.3389/fphys.2014.00130

Hashimoto N, Hamamura K, Kotani N, Furukawa Keiko, Kaneko K, Honke K, Furukawa Koichi. 2012. Proteomic analysis of ganglioside-associated membrane molecules: Substantial basis for molecular clustering. *Proteomics* **12**:3154–3163. doi:10.1002/pmic.201200279

Hirata M, Kamatani Y, Nagai A, Kiyohara Y, Ninomiya T, Tamakoshi A, Yamagata Z, Kubo M, Muto K, Mushiroda T, Murakami Y, Yuji K, Furukawa Y, Zembutsu H, Tanaka T, Ohnishi Y, Nakamura Y, Matsuda K, Shiono M, Misumi K, Kaieda R, Harada H, Minami S, Emi M, Emoto N, Arai H, Yamaji K,

Hiratsuka Y, Asai S, Moriyama M, Takahashi Y, Fujioka T, Obara W, Mori S, Ito H, Nagayama S, Miki Y, Masumoto A, Yamada A, Nishizawa Y, Kodama K, Kutsumi H, Sugimoto Y, Koretsune Y, Kusuoka H, Yoshiyama T. 2017. Cross-sectional analysis of BioBank Japan clinical data: A large cohort of 200,000 patients with 47 common diseases. *J Epidemiol* **27**:S9–S21. doi:10.1016/j.je.2016.12.003

Huang W-T, Chong I-W, Chen H-L, Li C-Y, Hsieh C-C, Kuo H-F, Chang C-Y, Chen Y-H, Liu Y-P, Lu C-Y, Liu Y-R, Liu P-L. 2019. Pigment epithelium-derived factor inhibits lung cancer migration and invasion by upregulating exosomal thrombospondin 1. *Cancer Lett* **442**:287–298. doi:10.1016/j.canlet.2018.10.031

Ishiura Y, Kotani N, Yamashita R, Yamamoto H, Kozutsumi Y, Honke K. 2010. Anomalous expression of Thy1 (CD90) in B-cell lymphoma cells and proliferation inhibition by anti-Thy1 antibody treatment. *Biochem Biophys Res Commun* **396**:329–334. doi:10.1016/j.bbrc.2010.04.092

Iwamaru Y, Kitani H, Okada H, Takenouchi T, Shimizu Y, Imamura M, Miyazawa K, Murayama Y, Hoover EA, Yokoyama T. 2016. Proximity of SCG10 and prion protein in membrane rafts. *J Neurochem* **136**:1204–1218. doi:10.1111/jnc.13488

Jiang S, Kotani N, Ohnishi T, Miyagawa-Yamguchi A, Tsuda M, Yamashita R, Ishiura Y, Honke K. 2012. A proteomics approach to the cell-surface interactome using the enzyme-mediated activation of radical sources reaction. *Proteomics* **12**:54–62. doi:10.1002/pmic.201100551

Jiao J, Sun K, Walker WP, Bagher P, Cota CD, Gunn TM. 2009. Abnormal regulation of TSG101 in mice with spongiform neurodegeneration. *Biochim Biophys Acta - Mol Basis Dis* **1792**:1027–1035. doi:10.1016/J.BBADIS.2009.08.009

Kanda Y. 2013. Investigation of the freely available easy-to-use software 'EZR' for medical statistics. *Bone Marrow Transplant* **48**:452–458. doi:10.1038/bmt.2012.244

Kaneko K, Ohkawa Y, Hashimoto N, Ohmi Y, Kotani N, Honke K, Ogawa M, Okajima T, Furukawa Keiko, Furukawa Koichi. 2016. Neogenin, Defined as a GD3-associated Molecule by Enzyme-mediated Activation of Radical Sources, Confers Malignant Properties via Intracytoplasmic Domain in Melanoma Cells. *J Biol Chem* **291**:16630–16643. doi:10.1074/jbc.M115.708834

Kim DI, Roux KJ. 2016. Filling the Void: Proximity-Based Labeling of Proteins in Living Cells. *Trends Cell Biol* **26**:804–817. doi:10.1016/j.tcb.2016.09.004

Koenig U, Sommergruber W, Lippens S. 2005. Aberrant expression of caspase-14 in epithelial tumors. *Biochem Biophys Res Commun* **335**:309–313. doi:10.1016/j.bbrc.2005.07.072

Kotani N, Gu J, Isaji T, Udaka K, Taniguchi N, Honke K. 2008. Biochemical visualization of cell surface molecular clustering in living cells. *Proc Natl Acad Sci* **105**:7405–7409. doi:10.1073/pnas.0710346105

Kotani N, Ida Y, Nakano T, Sato I, Kuwahara R, Yamaguchi A, Tomita M, Honke K, Murakoshi T. 2018. Tumor-dependent secretion of close homolog of L1 results in elevation of its circulating level in mouse model for human lung tumor. *Biochem Biophys Res Commun* **501**:982–987. doi:10.1016/j.bbrc.2018.05.096

Kotani N, Ishiura Y, Yamashita R, Ohnishi T, Honke K. 2012. Fibroblast Growth Factor Receptor 3 (FGFR3) Associated with the CD20 Antigen Regulates the Rituximab-induced Proliferation Inhibition in B-cell

Lymphoma Cells. *J Biol Chem* **287**:37109–37118. doi:10.1074/jbc.M112.404178

Kotani N, Yamaguchi A, Ohnishi T, Kuwahara R, Nakano T, Nakano Y, Ida Y, Murakoshi T, Honke K. 2019. Proximity proteomics identifies cancer cell membrane cis-molecular complex as a potential cancer target. *Cancer Sci* **110**:2607–2619. doi:10.1111/cas.14108

Krajewska M, Kim H, Shin E, Kennedy S, Duffy MJ, Wong YF, Marr D, Mikolajczyk J, Shabaik A, Meinhold-Heerlein I, Huang X, Banares S, Hedayat H, Reed JC, Krajewski S. 2005. Tumor-associated alterations in caspase-14 expression in epithelial malignancies. *Clin Cancer Res* **11**:5462–71. doi:10.1158/1078-0432.CCR-04-2527

Mikolajczyk J, Scott FL, Krajewski S, Sutherlin DP, Salvesen GS. 2004. Activation and Substrate Specificity of Caspase-14 †. *Biochemistry* **43**:10560–10569. doi:10.1021/bi0498048

Miyagawa-Yamaguchi A, Kotani N, Honke K. 2015. Each GPI-anchored protein species forms a specific lipid raft depending on its GPI attachment signal. *Glycoconj J* **32**:531–540. doi:10.1007/s10719-015-9595-5

Nagai A, Hirata M, Kamatani Y, Muto K, Matsuda K, Kiyohara Y, Ninomiya T, Tamakoshi A, Yamagata Z, Mushiroda T, Murakami Y, Yuji K, Furukawa Y, Zembutsu H, Tanaka T, Ohnishi Y, Nakamura Y, Kubo M, Shiono M, Misumi K, Kaieda R, Harada H, Minami S, Emi M, Emoto N, Daida H, Miyauchi K, Murakami A, Asai S, Moriyama M, Takahashi Y, Fujioka T, Obara W, Mori S, Ito H, Nagayama S, Miki Y, Masumoto A, Yamada A, Nishizawa Y, Kodama K, Kutsumi H, Sugimoto Y, Koretsune Y, Kusuoka H, Yanai H. 2017. Overview of the BioBank Japan Project: Study design and profile. *J Epidemiol* **27**:S2–S8. doi:10.1016/j.je.2016.12.005

Ohkawa Y, Momota H, Kato A, Hashimoto N, Tsuda Y, Kotani N, Honke K, Suzumura A, Furukawa Keiko, Ohmi Y, Natsume A, Wakabayashi T, Furukawa Koichi. 2015. Ganglioside GD3 Enhances Invasiveness of Gliomas by Forming a Complex with Platelet-derived Growth Factor Receptor α and Yes Kinase. *J Biol Chem* **290**:16043–16058. doi:10.1074/jbc.M114.635755

Raposo G, Stoorvogel W. 2013. Extracellular vesicles: Exosomes, microvesicles, and friends. *J Cell Biol*. doi:10.1083/jcb.201211138

Rees JS, Li X-W, Perrett S, Lilley KS, Jackson AP. 2015. Protein Neighbors and Proximity Proteomics. *Mol Cell Proteomics* **14**:2848–2856. doi:10.1074/mcp.R115.052902

Reithmeier RAF, Casey JR, Kalli AC, Sansom MSP, Alguel Y, Iwata S. 2016. Band 3, the human red cell chloride/bicarbonate anion exchanger (AE1, SLC4A1), in a structural context. *Biochim Biophys Acta - Biomembr* **1858**:1507–1532. doi:10.1016/j.bbamem.2016.03.030

Schey KL, Luther JM, Rose KL. 2015. Proteomics characterization of exosome cargo. *Methods* **87**:75–82. doi:10.1016/j.ymeth.2015.03.018

Shah R, Patel T, Freedman JE. 2018. Circulating Extracellular Vesicles in Human Disease. *N Engl J Med* **379**:958–966. doi:10.1056/NEJMra1704286

Soda M, Choi YL, Enomoto M, Takada S, Yamashita Y, Ishikawa S, Fujiwara S, Watanabe H, Kurashina K, Hatanaka H, Bando M, Ohno S, Ishikawa Y, Aburatani H, Niki T, Sohara Y, Sugiyama Y, Mano H. 2007. Identification of the transforming EML4–ALK fusion gene in non-small-cell lung cancer. *Nature* **448**:561–

566. doi:10.1038/nature05945

Soda M, Takada S, Takeuchi K, Choi YL, Enomoto M, Ueno T, Haruta H, Hamada T, Yamashita Y, Ishikawa Y, Sugiyama Y, Mano H. 2008. A mouse model for EML4-ALK-positive lung cancer. *Proc Natl Acad Sci* **105**:19893–19897. doi:10.1073/pnas.0805381105

Tauro BJ, Mathias RA, Greening DW, Gopal SK, Ji H, Kapp EA, Coleman BM, Hill AF, Kusebauch U, Hallows JL, Shteynberg D, Moritz RL, Zhu H-J, Simpson RJ. 2013. Oncogenic H-ras reprograms Madin-Darby canine kidney (MDCK) cell-derived exosomal proteins following epithelial-mesenchymal transition. *Mol Cell Proteomics* **12**:2148–59. doi:10.1074/mcp.M112.027086

Van de Craen M, Van Loo G, Pype S, Van Criekinge W, Van den brande I, Molemans F, Fiers W, Declercq W, Vandenabeele P. 1998. Identification of a new caspase homologue: caspase-14. *Cell Death Differ* **5**:838–846. doi:10.1038/sj.cdd.4400444

Van Niel G, D'Angelo G, Raposo G. 2018. Shedding light on the cell biology of extracellular vesicles. *Nat Rev Mol Cell Biol*. doi:10.1038/nrm.2017.125

Xu R, Rai A, Chen M, Suwakulsiri W, Greening DW, Simpson RJ. 2018. Extracellular vesicles in cancer — implications for future improvements in cancer care. *Nat Rev Clin Oncol* **15**:617–638. doi:10.1038/s41571-018-0036-9

Yamashita R, Kotani N, Ishiura Y, Higashiyama S, Honke K. 2011. Spatiotemporally-regulated interaction between β1 integrin and ErbB4 that is involved in fibronectin-dependent cell migration. *J Biochem* **149**:347–355. doi:10.1093/jb/mvq148

Yoshioka Y, Kosaka N, Konishi Y, Ohta H, Okamoto H, Sonoda H, Nonaka R, Yamamoto H, Ishii H, Mori M, Furuta K, Nakajima T, Hayashi H, Sugisaki H, Higashimoto H, Kato T, Takeshita F, Ochiya T. 2014. Ultra-sensitive liquid biopsy of circulating extracellular vesicles using ExoScreen. *Nat Commun* **5**:3591. doi:10.1038/ncomms4591